Electronic Supplementary Material (ESI) for Dalton Transactions.
This journal is © The Royal Society of Chemistry 2016

Electronic Supporting Information (ESI) for

^{1}H NMR spectroscopic Elucidation in Solution of the Kinetics and Thermodynamics of Spin Crossover for an exceptionally robust Fe^{2+} Complex

Holm Petzold,*[a)] Paul Djomgoue,[a)] Gerald Hörner,[b)] J. Matthäus Speck,[a)] Tobias Rüffer,[a)] and Dieter Schaarschmidt[a)]

a) TU Chemnitz, Institut für Chemie, Anorganische Chemie, Straße der Nationen 62, 09111 Chemnitz, Germany; Fax: +49-371-53137463; E-mail: holm.petzold@chemie.tu-chemnitz.de

b) TU Berlin, Institut für Chemie, Straße des 17. Juni 135, 10623 Berlin, Germany

Content

1 Supporting information

1.1 Syntheses of Ligands and Complexes

1.1.1 Syntheses of Ligands 5/6

1.1.1.1 Synthesis of N^1,N^2-*bis*(([2,2'-bipyridine]-6-yl)methyl)-*trans*-cyclohexane-1,2-diamine (*rac-trans*-***6***)

[2,2'-bipyridine]-6-carbaldehyde[1] (0.3 g, 1.6 mmol) was dissolved in dry EtOH (5 mL) and a solution of racemic *trans*-1,2-diaminocyclohexane (*rac-trans*-**4)** (0.092 g, 0.8 mmol) in dry EtOH (10 mL) was added dropwise to the reaction mixture. The mixture was stirred at room temperature under argon atmosphere for 5 min. Solid sodium borohydride (0.5 g, 9.61 mmol) was added during a period of 1 min time. The resulting colorless solution was stirred at room temperature for 5 min. The reaction was then quenched with water. The product was extracted tree times with CH_2Cl_2 (30 mL), dried over anhydrous Mg_2SO_4. After filtration, the solvent was evaporated to yield 0.27 g (0.56 mmol) of (*rac-trans*-**6**), 92 % from [2,2'-bipyridine]-6-carbaldehyde.[1] **^{1}H NMR** (500 MHz, $CDCl_3$) δ 8.64 (ddd, *J* = 4.8, 1.8, 1.2 Hz, 1H, *H*1), 8.39 (dt, *J* = 7.7, 1.0 Hz, 2H, *H*4), 8.24 (d, *J* = 7.3 Hz, 1H, *H*4'/6), 7.70 (t, *J* = 7.3 Hz, 1H, *H*5), 7.62 (dt, *J* = 7.7, 1.8 Hz, 1H, *H*3), 7.37 (d, *J* = 7.3 Hz, 1H, *H*4'/6), 7.23 (ddd, *J* = 7.7, 4.8, 1.2 Hz, 1H, *H*2), 4.14 (d, *J* = 14.3 Hz, 1H, *H*7), 3.95 (d, *J* = 14.3 Hz, 1H, *H*7), 2.45 – 2.41 (m, 1H, *H*8), 2.20 (d, *J* = 13.6 Hz, 1H, *H*9/10), 1.77 – 1.72 (m, 1H, *H*9/10), 1.30 – 1.26 (m, 1H, *H*9/10), 1.17 – 1.12 (m, 1H, *H*9/10).

1.1.1.2 Synthesis of N^1,N^2-*bis*(([2,2'-bipyridine]-6-yl)methyl)-N^1,N^2-dimethyl-*trans*-cyclohexane-1,2-diamine (*rac-trans-NMe*-**6**).

An aqueous solution of formaldehyde (2.29 mL, 37 %) was added to a solution of *rac-trans*-**6** (0.20 g, 0.46 mmol) in acetonitrile (acn) (4 mL) and a solution of acetic acid (4 mL) in acn (20 mL) was added and allowed to stir for 30 min. Subsequently sodium borohydride (0.047 g, 1.6 mmol) was introduced to that solution and the resultant mixture was stirred for a period of 24 h time. All solvents were removed and the

residue was made strongly basic with 3 M of aqueous sodium hydroxide in water. This aqueous mixture was extracted several times with CH_2Cl_2 (30 mL). Thereafter the combined organic phases were dried over magnesium sulfate and reduced to dryness to give *rac-trans-NMe*-**6** as a pale yellow oil; 0.18 g (0.36 mmol) 80 % from *rac-trans*-**6**. **^{1}H NMR** (500 MHz, $CDCl_3$): δ 8.64 (ddd, *J* = 4.8, 1.7, 1.2 Hz, 1H, *H*1), 8.35 (dt, *J* = 7.8, 1.2 Hz, 1H, *H*4), 8.20 (d, *J* = 7.6, 1H, *H*4'/6), 7.72 (t, *J* = 7.8 Hz, 1H, *H*5), 7.70 (td, *J* = 7.8 Hz, 1.7 Hz 1H, *H*3), 7.60 (d, *J* = 7.8 Hz, 1H, *H*4'/6), 7.24 (ddd, *J* = 7.8, 4.8, 1.2 Hz, 1H, *H*2). 4.04 (d, *J* = 14.4 Hz, 1H, *H*7), 3.88 (d, *J* = 14.4 Hz, 1H, *H*7), 2.74 – 2.68 (m, 1H, *H*8), 2.03 (m, 1H, *H*9/10), 1.76 (m, 1H, *H*9/10), 1.33 – 1.26 (m, 1H, *H*9/10), 1.23 (s, 3H, *NCH3*) 1.17 – 1.11 ppm (m, 1H, *H*9/10). **^{13}C NMR** (125.80 MHz, $CDCl_3$): δ 25.8 (*C10*), 35.05 (CH_3), 36.8 (*C9*), 60.4 (*C7*), 64.3 (*C8*), 119.0 (*C2*), 121.1 (*C6*), 123.0 (*C4'*), 123.4 (*C4*), 136.8 (*C12*), 137.0 (*C13*), 149.2 (*C3*), 155.1 (*C5*), 156.6 (*C1*), 160.7 ppm (*C11*).

1.1.1.3 Synthesis of N^1,N^2-*bis*((1,10-phenanthroline-2-yl)methyl)-*trans*-cyclohexane-1,2-diamine (*rac-trans*-**5a**).

Solid 1,10-phenanthroline-9-carbaldehyde **3**, (0.086 g, 0.4 mmol) was dissolved in dry EtOH (5 mL) and a solution of *trans*-1,2-diaminocyclohexane (*rac-trans*-**4**) (0.029 g, 0.2 mmol) was added dropwise. The reaction mixture was stirred at room temperature under argon atmosphere for 5 min. Thereafter solid sodium borohydride (0.5 g, 9.61 mmol) was added within 1 min and the resulting colorless solution was stirred at room temperature for 10 min. The reaction mixture was quenched with water. The mixture was extracted with CH_2Cl_2 (3x30 mL) and the combined organic phases dried with anhydrous Mg_2SO_4. After filtration, the filtrate was evaporated to dryness to yield *rac-trans*-**5a** as yellow oil, 0.035 g (0.07 mmol) 40 % from **3**. Purification of *rac-trans*-**5a** by column chromatography turned out to be extremely difficult due to the strong adsorption of the phenanthroline derivatives on common stationary phases and its sensitivity towards air. For these reasons, crude *rac-trans*-**5a** was used for complex synthesis as received. **^{1}H NMR** (500 MHz, $CDCl_3$): δ 9.08 (dd, *J* = 4.3, 1.7 Hz, 1H, *H*1), 8.15 (dd, *J* = 8.1, 1.7 Hz, 1H, *H*3), 8.04 (d, *J* = 8.2 Hz, 1H, *H*5), 7.87 (d, *J* = 8.2 Hz, 1H, *H*6), 7.66 (s, 2H, *H*4), 7.51 (dd, *J* = 8.1, 4.3 Hz, 1H, *H*2), 4.44 (d, *J* = 15.0 Hz, 1H, *H*7), 4.26 (d, *J* = 15.0 Hz, 1H, *H*7), 2.49 – 2.42 (m, 1H, *H*8), 2.19 (d, *J* = 13.2 Hz, 1H, *H*9/10), 1.68 – 1.62 (m, 1H, *H*9/10), 1.20 – 1.17 (m, 1H, *H*9/10), 1.08 – 1.01 ppm (m, 1H, *H*9/10). **^{13}C NMR** (125.80 MHz, $CDCl_3$): δ 25.0 (*C*10), 32.2 (*C*9), 53.4 (*C*7), 61.4 (*C*8), 122.4 (*C*2), 122.7 (*C*6), 125.5 (*C*4), 125.7 (*C*4), 126.4 (*C*14), 127.4 (*C*15), 128.7 (*C*3), 135.7 (*C*13), 135.9 (*C*12), 136.3 (*C*5), 150.1 (*C*1), 162.2 ppm (*C*11).

1.1.1.4 Synthesis of N^1,N^2-*bis*((1,10-phenanthroline-2-yl)methyl)-(*R*,*R*)-cyclohexane-1,2-diamine (*R,R-trans*-**5**) *and* N^1,N^2-*bis*((1,10-phenanthroline-2-yl)methyl)-(*S*,*S*)-cyclohexane-1,2-diamine (*S,S-trans*-**5**).

The pure enantiomers of the racemic mixture of rac-trans-**5** were synthesized in a similar manner using commercial available pure (*R*,*R*)-1,2-diaminocyclohexane (*R,R-trans*-**4**) and (*S*,*S*)-1,2-diaminocyclohexane (*S,S-trans*-**4**). The identity of *R,R-trans*-**5** and *S,S-trans*-**5** was confirmed by NMR spectroscopy.

1.1.1.5 Synthesis of N^1,N^2-*bis*((1,10-phenanthroline-2-yl)methyl)-*cis*-cyclohexane-1,2-diamine (*cis*-**5**).

The title compound N^1,N^2-bis((1,10-phenanthroline-2-yl)methyl)-*cis*-cyclohexane-1,2-diamine (*cis*-**5**) was prepared similar to *rac-trans*-**5**. **^{1}H NMR** (500 MHz, $CDCl_3$): δ 9.08 (dd, *J* = 4.3, 1.7 Hz, 1H, *H1*), 8.15 (dd, *J* = 8.1, 1.7 Hz, 1H, *H*3), 8.04 (d, *J* = 8.2 Hz, 1H, *H*5), 7.87 (d, *J* = 8.2 Hz, 1H, *H*6), 7.66 (s, 2H, *H*4), 7.51 (dd, *J* = 8.1, 4.3 Hz, 1H, *H*2), 4.44 (d, *J* = 15.0 Hz, 1H, *H*7), 4.26 (d, *J* = 15.0 Hz, 1H, *H*7), 2.49 – 2.42 (m, 1H, *H*8), 2.19 (d, *J* = 13.2 Hz, 1H, *H*9), 1.68 – 1.62 (m, 1H, *H*10), 1.20 – 1.17 (m, 1H, *H*10), 1.08 – 1.01 ppm (m, 1H, *H*9). **^{13}C NMR** (125.80 MHz, $CDCl_3$): δ 25.0 (*C*10), 32.2 (*C*9), 53.4 (*C*7), 61.4 (*C*8), 122.4 (*C*2), 122.7 (*C*6), 125.5 (*C*4), 125.7 (*C*4), 126.4 (*C*14), 127.4 (*C*15), 128.7 (*C*3), 135.7 (*C*13), 135.9 (*C*12), 136.3 (*C*5), 150.1 (*C*1), 162.2 ppm (*C*11).

1.1.1.6 Synthesis of N^1,N^2-*bis*((1,10-phenanthroline-2-yl)methyl)-N^1,N^2-dimethyl-*trans*-cyclohexane-1,2-diamine (*rac-trans-NMe*-**5a**).

To a solution of *rac-trans*-**5** (0.32 g, 0.64 mmol) in acetonitrile (30 mL) acetic acid (10 mL) was added and the solution stirred for one hour. Aqueous formaldehyde (37%, 3.35 mL) was added and stirring was continued overnight, thereafter $NaBH_4$ (0.4 g, 10.57 mmol) was added to the solution. More $NaBH_4$ (0.4 g, 10.57 mmol) was introduced after 5 h and stirring continued overnight. Water was added and the product was extracted with CH_2Cl_2 (3x30 mL). The product was purified by column chromatography using Al_2O_3 and THF/MeOH in the ratio 10/0.5, yield 0.2 g (0.38 mmol), 63 % from *rac-trans*-**5**. **^{1}H NMR** (500 MHz, $CDCl_3$): δ 9.07 (dd, *J* = 4.3, 1.7 Hz, 1H, *H*1), 8.14 (dd, *J* = 8.1, 1.7 Hz, 1H, *H*3), 8.03 (d, *J* = 8.2 Hz, 1H, *H*5), 7.84 (d, *J* = 8.2 Hz, 1H, *H*6), 7.64 (s, 2H, H4), 7.50 (dd, *J* = 8.1, 4.3 Hz, 1H, *H*2), 4.55 (d, *J* = 15.3 Hz, 1H, *H*7), 4.35 (d, *J* = 15.3 Hz, 1H, *H*7), 2.65 (m, 1H, *H*8), 2.23 (m, *J* = 10.0 Hz, 1H, *H*9), 1.67 (d, *J* = 6.3 Hz, 1H, *H*10), 1.17 (s, 3H, *NCH3*),

1.16 – 1.13 (m, 1H, *H*10), 0.85 – 0.72 ppm (m, 1H, *H*9). **^{13}C NMR** (125.80 MHz, $CDCl_3$): δ 25.8 (*C*10), 29.67 (*C*9), 36.8 (CH_3), 60.41 (*C*7), 64.32 (*C*8), 120.0 (*C*2), 121.2 (*C*6), 123.0 (*C*4), 123.45 (*C*4), 136.85 (*C*14), 137.1 (*C*15), 137.6 (*C*3), 149.3 (*C*13), 155.1 (*C*12), 156.6 (*C*5), 158.7 (*C*1), 160.8 ppm (*C*11).

1.1.2 General Synthesis of Complexes from hexadentate Ligands

The appropriate ligands **5** or **6** (0.14 mmol) and $FeSO_4{\cdot}7H_2O$ (38.9 mg, 0.14 mmol) were stirred in absolute ethanol (5 mL) for 2 h; 5 mL of acn was added to the solution. After addition of NH_4PF_6 (150mg), the intensively colored solution was stirred for 1 h. A precipitate formed after addition of 5 mL of isopropanol. The precipitate was collected by centrifugation and washed with isopropanol. Water (20mL) and acn (5 mL) were added and the mixture was extracted twice with dichloromethane (2 x 20 mL). The organic layer was dried over $MgSO_4$ and the solid complex was obtained after taking the solvent to dryness. The purification of the complex was achieved by dissolving the complex in a small volume of acn and subsequent addition of larger amounts of isopropanol. The solvent volume was reduced slowly using a rotary evaporator until a precipitate starts to form. At this point the reaction mixture was placed in a fridge overnight and the precipitate was collected by centrifugation. These steps were repeated several times. Complexes employing the counter ions $(ClO_4)^-$ and $(BF_4)^-$ were prepared without counter ion exchange by using $[Fe(OH_2)_6](ClO_4)_2$ and $[Fe(OH_2)_6](BF_4)_2$, respectively.

[Fe(*rac-trans-NMe*-**6**)]$(BF_4)_2$ Anal. calcd. for $C_{30}H_{34}B_2F_8FeN_6{\cdot}H_2O$(%) C: 49.62, H: 5.00, N: 11.57 found. C: 49.52, H: 5.06 N: 11.29; **^{1}H NMR** (500 MHz, d_5-nitrobenzene, 300 K): δ 8.80 (d, *J* = 8 Hz, 1H, *H*4'), 8.54 (d, *J* = 8.0 Hz, 1H, *H*4), 8.40 (t, *J* = 8Hz, 1H, *H*5), 8.01 (d, *J* = 8.0 Hz, 1H, *H*6), 7.94 (dt, *J* = 8.0/1.2 Hz, 1H, *H*3), 7.13 (ddd, *J* = 7.8/5.6/1.5 Hz, 1H, *H*2), 6.74 (d, *J* = 5.6 Hz, 1H, *H*1), 4.36 (d, J = 16.5 Hz, 1H, *H*7-1), 3.17 (d, J = 16.5 Hz, 1H, *H*7-2), 2.28 (m, 1H, cyc-hexyl), 2.05 (m, 1H, cyc-hexyl), 1.63 (m, 1H, cyc-hexyl), 1.12 (m, 1H, cyc-hexyl), 1.01 ppm (m, 1H, cyc-hexyl); **FTIR**: ν/cm^{-1} (KBr disc): 3431(s), 3300(m), 3001(m), 2985(m), 2895(m), 1653(m), 1577(w), 1454(s), 1398(w), 1098(w), 856(s), 740(m), 533(s). **ESI-MS**(CH_2Cl_2/acn): *m/z* calcd. for [Fe(*rac-trans-NMe*-**6**)$(BF_4)_2$ + Na]$^+$: 731.2156 found 731.2127.

[Fe(*rac-trans*-**5**)]$(PF_6)_2$, Anal. Calcd. for $C_{32}H_{30}F_{12}FeN_6P_2{\cdot}$(0.5 *i*PrOH) (%) C: 46.01, H: 3.92, N: 9.61 found C: 46.41, H: 4.11, N: 9.75; **^{1}H NMR** (500 MHz, d_3-acn, 300 K): δ 19.17 (bs, LW = 210 Hz, 1H, *H*1), 15.19 (bs, LW = 150 Hz, 1H, *H*7-1), 13.25 (bs, LW = 30 Hz, 1H, *H*6), 10.65 (bs, LW = 16 Hz, 1H, *H*2), 9.50(m, 2H, *H*3/*H*4), 9.20 (d, *J* = 8.6Hz, 1H, *H*3), 7.03 (s, LW = 13 Hz 1H, *H*7-2), 6.78 (d, *J* = 7 Hz, 1H, *H*5), 4.59(bs, LW = 30 Hz, 1H ,*H*8), 3.98 (bs, LW = 70 Hz, 1H, N*H*), 3.73 (d, *J* = 10 Hz, 1H, *H*9), 3.12 (d, J = 6 Hz, 1H,

*H*10(eq.), 1.85 (bs, 1H, *H*9), 1.57 (t, *J* = 9 Hz, 1H, *H*10(ax.)); **FTIR**: *ν*/cm^{-1} (KBr disc) 3431(s), 3302(m), 3090(m), 2985(m), 2938(m) 1653(m), 1628(m), 1577(w), 1455(s), 1512(w) 1433(w), 1050(w), 850(s), 744(m), 540(s). ESI-**MS**(CH_2Cl_2/acn) m/z calcd. for [Fe(*rac-trans*-**5**)ClO_4)-2H]$^+$: 651.1205 found 651.1222 (Imine-formation); calcd. for [Fe(*rac-trans*-**5**)ClO_4)]$^+$: 653.1321 found 653.1321.

[Fe(*R*,*R-trans*-**5**)]$(ClO_4)_2$: Anal. Calcd for $FeC_{32}H_{30}N_6Cl_2O_8{\cdot}0.5H_2O$ $0.5CH_2Cl_2$ (%) C: 48.50, H: 4.01, N: 10.44 found C: 48.63, H: 3.87, N: 10.94. *ν*/cm^{-1} (KBr disc) 3421(s), 3255(m) 3090(m), 2929(m), 2958(m), 1617(m), 1589(m), 1508(w), 1455(s), 1512(w), 1452(w), 1427(w), 1397(w), 1092(w), 851(m), 734(w), 724(w), 624(s).

[Fe(*rac-trans-NMe*-**5**)]$(BF_4)_2$: Anal. calcd for $C_{34}H_{34}B_2F_8FeN_6{\cdot}H_2O$ (%) C: 52.75, H. 4.69, N: 10.86 found C: 52.72, H.4.74, N: 10.63. **^{1}H NMR** (500 MHz, d_3-acn, 300 K): δ 9.81 (bs, LW = 34 Hz, 1H, *H*1), 9.53 (d, LW = 5 Hz, *J* = 8.5 Hz, 1H, *H*6), 8.66 (m, 2H, *H*4/*H*3), 8.56 (d, LW < 5 Hz, *J* = 9.0 Hz, 1H, *H*4), 8.36 (d, LW < 5 Hz, *J* = 9Hz, 1H, *H*5), 8.14 (d, LW = 10 Hz, 6.5Hz, *H*2), 7.11 (d, LW = 12 Hz, *J* = 12Hz, 1H, *H*7-1), 4.01 (d, LW = 8 Hz, *J* = 17Hz, 1H, *H*7-2), 3.41 (bs, LW = 20 Hz, 1H, *H*8), 2.72 (bs, LW = 30 Hz, 3H, Me), 2.41 (d, LW = 8 Hz, *J* = 12.5Hz, 1H, cyc-hexyl), 2.07 (m, 1H, cyc-hexyl) 1.38 (bm, 1H, cyc-hexyl), 1.23 ppm (t, *J* = 9.5Hz, 1H, cyc-hexyl); **FTIR**: *ν*/cm^{-1} (KBr disc) 3409(s), 3050(m), 2937(m), 2865(w) 1653(m), 1576(m), 1420(w), 1395(w), 11364(m) 1295(m), 1212(w), 1061(s), 860(m), 734(w), 725(w), 575(w). **ESI-MS** (CH_2Cl_2/acn) *m/z* calcd. for [Fe(*rac-trans-NMe*-**5**)]$^{2+}$: 291.1092 found 291.1157; calcd. for [Fe(*rac-trans-NMe*-**5**)-H$^+$]$^+$: 581.2116; found 581.2111.

[Fe(*cis*-**5**)]$(ClO_4)_2$: Anal. calcd for $C_{32}H_{30}Cl_2FeN_6O_8{\cdot}0.5\ H_2O$ $0.5\ CH_2Cl_2$ (%) C: 48.50, H: 4.01, N: 10.44 found C: 48.63, H: 3.87, N: 10.94. **^{1}H NMR** (500 MHz, d_5-nitrobenzene, 373 K): δ 141.9 (LW = 500 Hz, 1H), 129.5 (LW = 500 Hz, 1H), 116.1 (LW = 500 Hz, 1H), 107.2 (LW = 450 Hz, 1H), 91.1 (LW = 280 Hz, 1H), 57.1 (LW = 220 Hz, 1H), 56.8 (LW = 220 Hz, 1H), 46.0 (LW = 370 Hz, 1H), 43.2 (LW = 80 Hz, 1H), 42.2 (LW = 60 Hz, 1H), 39.8 (LW = 220 Hz, 1H), 38.4 (LW = 50 Hz, 1H), 30.4 (LW = 700 Hz, 1H), 26.8 (LW = 500 Hz, 1H), 23.4 (LW = 120 Hz, 1H), 21.9 (LW = 20 Hz, 1H), 20.9 (LW = 20 Hz, 1H), 18.8 (LW = 50 Hz, 1H), 18.6 (LW = 15 Hz, 1H), 18.2 (LW = 15 Hz, 1H), 17.8 (LW = 15 Hz, 1H), 15.1 (LW = 12 Hz, 1H), 14.1 (LW = 34 Hz, 1H), 9.5 (LW = 70 Hz, 1H), 8.0 (LW = 20 Hz, 1H), 6.4 (LW = 20 Hz, 1H), 3.4 (LW = 25 Hz, 1H), -5.07 (LW = 350 Hz, 1H), –9.0 (LW = 30 Hz, 1H), –13.1 ppm (LW = 30 Hz, 1H); **FTIR**: (KBr) cm^{-1}: 3425(s), 3260 (m) 3092(m), 2930(m), 2970(m), 1615(s), 1590(m), 1509(w), 1455(s), 1514(m), 1450(m), 1425(w), 1398(w), 1095(w), 850(m), 733(w), 725(w), 626(s). **ESI-MS** (CH_2Cl_2/acn) *m/z* calcd. for [Fe(*cis*-**5**) (ClO_4)]$^+$: 653.1366 found 653.1244.

[Zn(*S*,*S*-*trans*-**5**)]$(ClO_4)_2$: $Zn(H_2O)_6(ClO_4)_2$ (750 mg, 0.2 mmol) was added to a solution of *S*,*S*-*trans*-**5** (100mg, 0.2 mmol) in ethanol. The solution was stirred and refluxed for 40 min resulting in a precipitate. This precipitate was isolated by centrifugation and washed 3 times with ethanol to obtain the pure compound. [Zn(*S*,*S*-*trans*-**5**)]$(ClO_4)_2$ Anal. Calcd for $C_{32}H_{30}Cl_2N_6O_8Zn{\cdot}H_2O$ (%) C: 49.22, H: 4.13, N: 10.76 found C: 48.46, H: 3.82, N: 10.64. **^{1}H NMR** (d_3-acn, 500 MHz): δ 8.97 (d, *J* = 8.2 Hz, 1H, *H*5), 8.65 (dd, *J* = 8.2, 1.4 Hz, 1H, *H*3), 8.31 (d, *J* = 9.0 Hz, 1H, *H*4/4'), 8.20 (d, *J* = 9.0 Hz, 1H, *H*4/4'), 8.17 (d, *J* = 8.2 Hz, 1H, *H*6), 8.04 (dd, *J* = 4.7, 1.4 Hz, 1H, *H*1), 7.68 (dd, *J* = 8.2, 4.7 Hz, 1H, *H*2), 4.60 (d, *J* = 17.8 Hz, 1H, *H*7), 4.53 (dd, *J* = 17.8, 6.0 Hz, 1H, *H*7), 3.21 (dd, *J* = 10.8, 5.6 Hz, 1H, *H*8), 2.18 – 2.11 (dt, *J* = 10.5 Hz, 1H, *H*9/10), 1.67 – 1.61 (dt, *J* = 10.5, 5.6 Hz, 1H, *H*9/10), 1.09 (dt, *J* = 10.5, 5.6 Hz,, 1H, *H*9/10), 0.98 – 0.90 ppm (dt, *J* = 10.5 Hz, 1H, *H*9/10). **^{13}C NMR** (d_3-acn, 126 MHz): δ 24.96 (*C*10), 45.99 (*C*9), 56.18 (*C*7), 58.06 (*C*8), 123.44 (*C*2), 124.61 (*C*6), 125.17 (*C*4), 126.21 (*C*4), 127.09 (*C*14), 128.83 (*C*15), 128.87 (*C*3), 139.05 (*C*13), 139.21 (*C*12), 139.34 (*C*5), 156.58 (*C*1), 157.32 ppm (*C*11). **ESI-MS** (CH_2Cl_2/acn) m/z calcd for [Zn(*S*,*S*-*trans*-**5**)] $(ClO_4)]^+$ 661.1303, found 661.1281.

1.1.3 Preparation of Epoxy-Samples

The compounds [Fe(*rac*-*trans*-**5**)]$(PF_6)_2$ and [Fe(*rac*-*trans*-*NMe*-**5**)]$(PF_6)_2$ were embedded in commercial available cast resin (epoxy resin and hardener L from R&G Faserverbundwerkstoffe GmbH) by dissolving the compounds with gentle heating of 2 mg complex in 2 g hardener. Immediately after dissolution the hardener and resin were mixed as indicated by the manufacture and larger portions were placed on microscope slides. The samples were allowed to stand for 2h at ambient temperature. After that period a lid was place on the top and a little shim was placed between slide and lid to keep the distance in the desired distance. After 1-2d the resin fully hardened.

1.2 Solvatochromism

Solvent dependent spectra were recorded using a thermos electron corporation Genesys 6 spectrometer with quartz cuvettes (d = 0.01 m) with sample concentrations of 1 mM. Solvatochromism spectra were recorded at ambient temperature. The results are shown in Figure 1-SI and Figure 2-SI.

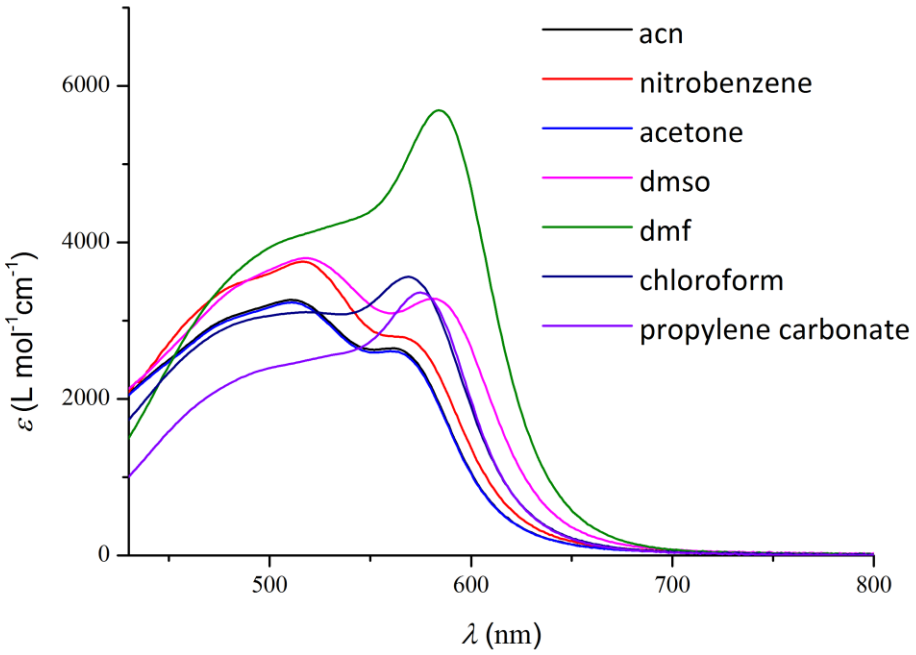

Figure 1-SI: UV/vis spectra of the complex [Fe(rac-*trans*-**5**)]$^{2+}$ in various solvents.

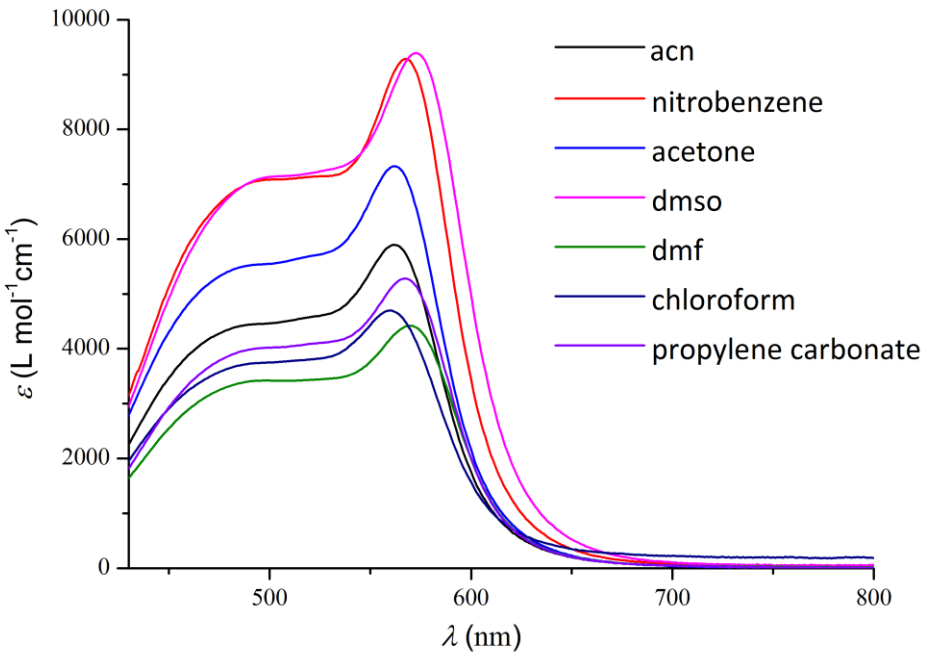

Figure 2-SI: UV/vis spectra of the complex [Fe(rac-*trans*-*NMe*-**5**)]$^{2+}$ in various solvents.

Table 1-SI: Data for the MLCT transition at the lowest energy in electronic spectra of [Fe(*rac-trans*-**5**)]$(PF_6)_2$ and [Fe(*rac-trans-NMe*-**5**)]$(BF_4)_2$ in different solvent.

	solvent	acn	nitro-benzene	acetone	dmso	dmf	$CHCl_3$	propylen carbonate
[Fe(*rac-trans-NMe*-**5**)]$(BF_4)_2$	ε_{max} (L/mol·cm)	5900	9300	7300	9300	4400	4700	5300
	λ_{max} (nm)	562	568	562	575	569	560	567
[Fe(*rac-trans*-**5**)]$(PF_6)_2$	ε_{max} (L/mol·cm)	3300	3800	2600	3800	5700	3100	3400
	λ_{max} (nm)	560	566	560	584	585	569	575

The methylated complex [Fe(*rac-trans-NMe*-**5**)]$^{2+}$ shows weaker solvatochromism (from 560 nm ($CHCl_3$) to nm 575 nm (dmso)) than complex [Fe(*rac-trans*-**5**)]$^{2+}$ (from 560 nm (acetone) to 585 nm (dmso)). In addition the ratios of the intensities for the CT absorptions in the visible region are strongly dependent on the solvent for [Fe(*rac-trans*-

5)]$^{2+}$ but constant for [Fe(*rac-trans-NMe-***5**)]$^{2+}$ (see Figure 1-SI and 2-SI). As solvatochromism is typical for CT absorptions and is a measure for the reorganization of the solvent cage associated with the charge transfer, this finding is (assumed from the main paper) consistent with a higher shielding of the metal center by the methyl group which reduces the influence of the solvent and hinders the formation of hydrogen bonds.

1.3 General Remarks on NMR Spectroscopic Methods

The aim of the following section is to outline the NMR methods developed and used throughout the study. In particular, NMR is used to obtain the SCO thermodynamics from the chemical shifts as well as the SCO kinetic parameters from the linewidths and relaxation time measurements. The methods are based on well-known models used in paramagnetic NMR spectroscopy. All calculations were made by using the equations nicely assembled in the text book of Bertini[2]. For completeness, all relevant equations are compiled in this supporting information. Most of the curve fitting was done with the Origin program package. For the simultaneous curve fitting of the chemical shifts of many protons (C^1 and global $\Delta_{SCO}H$ and $\Delta_{SCO}S$), a homemade Excel program was used that allows straightforward data processing and handling. As this program is not yet able to calculate standard errors, the results are given without standard errors and are only judged by comparing calculated and experimental chemical shifts. Standard errors are given in parenthesis if the Origin package was used; confidence intervals of 99.7% are given with preceding ±. The sample temperature in the probe head of the NMR spectrometer was corrected by a calibration curve obtained using methanol or glycol samples, as described in the literature.[3,4] For very accurate measurements, a small volume of anhydrous methanol or glycol was placed with an inset tube in the middle of the NMR tube and used to calculate the sample temperature according to reported calibration curves[3,4].

1.4 Variable Temperature ^{1}H NMR Spectroscopy

1.4.1 Simplifications Applied

For the calculation of linewidths and relaxation rates the following simplifications were applied.

a) Only dipolar contributions to the nuclear relaxation rates R_1 and Curie relaxation were taken into account.

b) Contact relaxation was neglected; the validity was checked by rough calculations.

c) All protons were treated as being independent without the possibility of cross relaxation.

d) Only the Fe-atom was treated as a relaxation source.

e) Relaxation processes in the LS state were neglected.

f) Susceptibility was treated as if isotropic with $g = g_e$

1.4.2 Notation of the Proton Sites in the Complexes [Fe(5/6)]$^{2+}$.

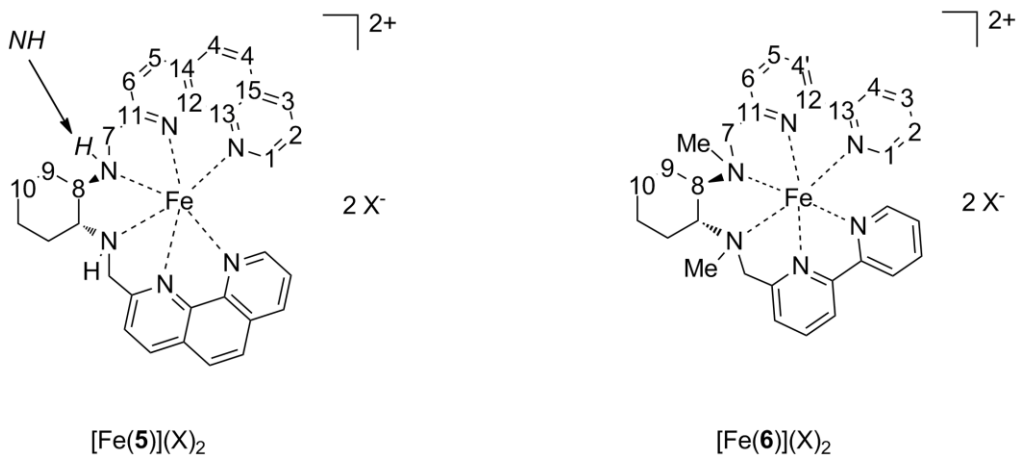

Figure 3-SI: Position numbering scheme for protons and carbon used in discussion of NMR spectra and compound characterization.

Data acquisition and processing was done with standard pulse sequences and software included in TopSpin 2.1 program package on a Bruker Avance III 500 MHz spectrometer. The initial assignment of the NMR signals of the Fe^{2+} complexes [Fe(*rac-trans*-**5**)]$^{2+}$, [Fe(*rac-trans-NMe*-**5**)]$^{2+}$ and [Fe(**6**)]$^{2+}$ was based on the coupling pattern and ^1H-^1H-COSY spectroscopy at low temperature and classical assignment rules. It turned out to be difficult to assign the protons *H*8, *H*9 and *H*10 in the cyclohexyl fragment and the CH_2 protons *H*7 as well as the proton *H*4. Assignment of the two protons *H*4 (in [Fe(**5**)]$^{2+}$) was not unambiguously possible and therefore those two protons where treated together as *H*4-1 and *H*4-2. In order to assign *H*8 to *H*10 and to distinguish between the two CH_2-protons *H*7-1 and *H*7-2, the longitudinal relaxation times T_1 were analyzed. The approximation $R_1 = 1/T_1 \sim 1/r^6$ (r being the distance

between Fe^{2+} ion and H atom) was used for the assignment (Figure 21-SI and Table 10-SI). Intramolecular distances between a proton site and the iron ion were approximated with respective Zn···H distances taken from the molecular structure of the zinc complex [Zn(*rac-trans*-**5**)]$(ClO_4)_2$, obtained via x-ray single-crystal structure analysis,

1.4.3 High field Shift of Proton H5

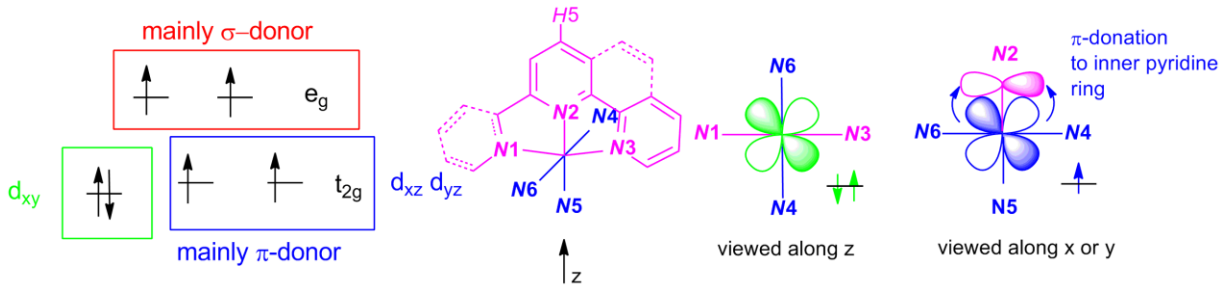

Figure 4-SI: The proton *H*5 is the only proton that is shifted to high field in the HS state; this can be explained by a preferred localization of paired *d*-electron density in the d_{xy} orbital. In consequence, unpaired electron density is only donated through *N*5 and *N*2 into the π-system of the two inner pyridine rings. This causes high field shift of *H*5 in the para-position. (Coloring indicted the affiliation of a particular terpy- or related ligand)

In aromatic ligands like pyridine bonded to a paramagnetic metal, the contact coupling δ^{con} can be subdivided into contributions mainly transmitted through the σ-donor orbitals ($\delta^{\sigma\text{-con}}$) and those transmitted through the π-back donation ($\delta^{\pi\text{-con}}$). Direct coupling of unpaired electrons with the 1s-orbital of the proton causes shifts of the resonance down-field with respect to the diamagnetic shift. In the complexes discussed in this contribution, almost all resonances of aromatic protons shift down-field, pointing to dominant $\delta^{\sigma\text{-con}}$ contributions. The only exception is *H*5; -this behaviour is typical for protons in the para position of the inner pyridine ring of HS-[Fe^{2+}(terpy)$_2$] complexes (terpy = 2,2′:6′,2′′-terpyridine) and related complexes. This behaviour points to a ground state of the HS-Fe^{2+} complex having the only paired electrons in a *d*-orbital located between the two meridional ligands, or two arms in case of

[Fe(**5**/**6**)$^{2+}$. With this configuration, π-back donation is only possible into the π-system of the inner pyridine ring; for further explanation see Figure 4-SI.

Apart from the high field shift of proton *H*5, it is difficult to figure out which contribution for a given 3d-metal complex actually dominates the chemical shift. In a first order approximation, δ^{pc} and $\delta^{\sigma\text{-con}}$ are dominating the chemical shifts of protons close to the paramagnetic metal. Due to the larger delocalization in aromatic π-system, the contact coupling $\delta^{\pi\text{-con}}$ can give sizable contributions to the chemical shifts for protons far away from the metal.

1.4.4 Determination of Thermodynamic Parameters $\Delta_{SCO}H$, $\Delta_{SCO}S$ and $T_{1/2}$

1.4.4.1 *Linear Expansion of the Curie Constants C: Justification*

In proton NMR spectroscopy of paramagnetic transition metal complexes, the paramagnetic contribution δ_{para} to the chemical shift can be assigned to two main sources: a) the contact coupling δ^{con} which arises from spin density in the 1s-orbital of the hydrogen atom and b) the dipolar contribution; so-called pseudo-contact coupling δ^{pc} arising from dipolar coupling between the paramagnetic metal centre and the proton magnetic moment. Both contributions can shift the resonance down or up-field. The paramagnetic contribution to the chemical shift can be calculated from coupling constants A^{pc} and A^{con} by equations (1) and (2) with appropriate Lande factors g (g_e for δ^{con} and $\bar{g}$ for δ^{pc}).

$$\delta^{pc/con} = \frac{A^{pc/con}}{\hbar}\frac{g\mu_B S(S+1)}{3\gamma_I kT} = \frac{C}{T} \quad \text{(S = 2 for HS-Fe}^{2+}\text{)} \qquad (1)$$

$$C = \frac{A^{pc/con}}{\hbar}\frac{g\mu_B S(S+1)}{3\gamma_I k} \qquad (2)$$

In a first order approximation, both hyperfine-coupling constants A^{pc} and A^{con} are temperature independent. Hence the chemical shifts behave Curie-like (Curie constant *C*).[5] In practice, octahedral Fe^{2+} complexes have low lying exited states with electron density redistributed within the 3d-orbitals.[6] These low lying exited states are populated thermally. For instance, the quintet ground state of ideal octahedral complexes is triply degenerate. These three states will split into three individual levels under reduced symmetry. Similar effects arise from zero field splitting.[2]

$$\gamma_{HS}(T) = \frac{1}{1 + e^{\frac{\Delta_{SCO}H}{R}\left(\frac{1}{T} - \frac{1}{T_{½}}\right)}} = \frac{1}{1 + e^{\frac{\Delta_{SCO}H}{R}\left(\frac{1}{T} - \frac{\Delta_{SCO}S}{\Delta_{SCO}H}\right)}} \qquad (3)$$

We can conclude that, in addition to the ground state coupling constant A, various additional coupling constants of exited states $A^*{}_{1,2,\ldots}$ have to be taken into account for the effective coupling constant observed at a given temperature. Here we use $\bar{A}(T) = a_1\, A^*{}_1 + a_2\, A^*{}_2 \cdots$, with $a_1, a_2 \cdots$ being the mole fractions of the various states in the thermal equilibrium. Similar to the HS/LS equilibrium, the populations of the ground state and exited states within the quintet manifold can be described by a Boltzmann distribution.[6] At variance with the HS/LS equilibrium, the entropic differences between ground and various exited states of the HS-state are small enough to be neglected. This simplification is justified: a) all exited states belong to the quintet manifold with *S* = 2; b) they will exhibit similar Fe-L bond strength (redistribution of electrons between nonbonding and antibonding d-orbitals is unlikely due to the high energy that is needed). For these reasons, the entropy changes only slightly between ground and exited state. In consequence, the transitions between ground and exited state(s) within the HS-configuration (S = 2) will be extremely gradual. In particular, it will be negligible for smaller temperature ranges around and above ambient temperature. In these cases, $\bar{A}(T)$ and $C(T)$ appear temperature independent. In addition, the most sizable contribution to all coupling constants (*vide infra*) of a proton close (< 5 Å) to the paramagnetic metal is caused by *σ*-contact coupling. Hence, the difference between A and $A^*{}_{1,2,\ldots}$, caused by different distributions of the electrons within the nonbonding d-orbitals, effecting only π-contact coupling, will be small. Therefore the average $\bar{A}(T)$, and subsequently also $\bar{C}(T)$, can be safely approximated by equation (4).

$$C(T) = C^0 + C^1 T \quad (4)$$

The mathematical description of the population of exited states within the HS state and the distribution between the HS- and LS-state (SCO equilibrium) are closely related. Therefore, for the majority of cases even a fit assuming a temperature independent Curie constant C^0 will yield reasonable agreement of the calculated and the experimental results for a particular proton. The resulting systematic error in $\Delta_{SCO}H$ and $\Delta_{SCO}S$ is often small enough to be neglected.

On the other hand, real HS-Fe^{2+} complexes will often show obvious deviations from the ideal Curie behaviour. To account for this, it is possible to fit the chemical shift of HS-Fe^{2+} complexes by explicit fitting of *A*(T), or likewise *C*(T), on a Boltzmann distribution between the ground and one or more exited states. This was demonstrated for static paramagnetic complexes[6,7] and Fe^{2+}-SCO complexes[8–11] by Weber, Walker and Shokhirev. However, in the case of SCO complexes with an additional HS/LS equilibrium, it is hard to obtain experimental data that allow a fit of the experimental data to yield reasonable results for the energy gap and couplings constants not only by chance. For example, with a typical value of C^0 in the range of 40000 ppm K, the chemical shifts of the protons in the HS-species will vary by $d\delta/dT = C^0 \frac{1}{T^2}$ (about 0.5 ppm/K at ambient temperature). In practice, the sample temperature in the probe head can be measured not more precisely than 0.1 K. It either requires long waiting times to equilibrate the sample or the use of internal standards to achieve this accuracy for all recorded spectra. Realistically the accuracy is not better than 0.3 K, especially over larger temperature ranges. Thus we can expect an accordance of the experimental data with calculated data by 0.15 ppm difference for the HS species. In addition, the HS/LS equilibrium also shifts the resonances with changing temperature up to 0.6 ppm/K. Altogether, an approximation of *C*(*T*) according to equation (4) is a meaning- and powerful compromise in the light of experimental available accuracy. All higher term terms can be neglected.

1.4.5 Classical Fitting with Temperature Independent Curie Constants

All spectra were referenced internally to peaks of residual protons in the deuterated solvents.[12] The reference for nitrobenzene was set as to obtain 0 ppm for tetramethylsilane. The chemical shifts $\delta_{dia/LS}$ for the LS species in d_7-dmf and d_5-pyridine were estimated by initial free refinement with reasonable values of $\Delta_{SCO}H$ and $\Delta_{SCO}S$. Due to the fact that the HS fraction at the lowest available temperature is very small, errors in $\Delta_{SCO}H$ and $\Delta_{SCO}S$ do not contribute considerably to $\delta_{dia/LS}$. In solvents that solidify at temperatures that are too high to allow obtaining $\delta_{dia/LS}$(such as d_5-nitrobenzene), the diamagnetic contribution to the chemical shifts $\delta_{dia/LS}$ were approximated from data retrieved from the d_7-dmf solutions. The diamagnetic contributions δ_{LS} and δ_{dia} were set equal and termed $\delta_{dia/LS}$. No attempts were made to correct $\delta_{dia/LS}$ for solvent effects. The term δ_{dia} gives the hypothetical chemical shift of the HS state without paramagnetic contribution, while the term δ_{LS} gives the chemical shift of the LS state. While δ_{dia} and δ_{LS} are not identical, often corresponding zinc complexes are used to estimate δ_{dia}. As an example, Table 2 compiles the observed chemical shifts of [Fe(*rac-trans*-**5**)]$^{2+}$ at 323 K, δ_{LS} extracted by extrapolation by using observed chemical shifts as well as the chemical shifts observed for the zinc analogue [Zn(*rac-trans*-**5**)]$^{2+}$. Larger differences are found only for proton *H*1 and *H*7-1 and *H*7-2. The sizeable difference for *H*1 can be explained by the specific position in a shielded region of the π-system of the phenanthroline group. The smaller ion radius of *ls*-Fe^{2+} ion forces *H*1 closer by 0.24 Å to the π-system of the phenanthroline group and hence shifts *H*1 downfield. Altogether the differences are small enough to set δ_{dia} and δ_{LS} to the same value. This approach also stabilises the refinement and avoids over-parameterization.

Table 2-SI: Compilation of selected chemical shifts of [Zn(*rac-trans*-**5**)]$^{2+}$ [Fe(*rac-trans*-**5**)]$^{2+}$ (at 232 K) in d_3-acn solution and the calculated chemical shift for the LS state of [Fe(*rac-trans*-**5**)]$^{2+}$.

Proton/ d_3-acn	[Zn(*rac-trans*-**5**)]$^{2+}$ δ_{obs} (ppm)	[Fe(*rac-trans*-**5**)]$^{2+}$ (232 K) δ_{obs} (ppm)	[Fe(*rac-trans*-**5**)]$^{2+}$ δ_{LS} (ppm) (calcd)
*H*1	8.03	7.46	7.00
*H*2	7.67	7.51	7.39
*H*3	8.65	8.54	8.50

*H*4/*H*4'	8.20 / 8.30	8.35 / 8.60	8.31 / 8.57
*H*5	8.97	8.93	9.03
*H*6	8.17	8.61	8.43
*H*7-1/*H*7-2	4.53 / 4.60	4.95 / 3.90	4.55 / 3.77

In order to prepare data for the fitting, the $y_{HS}(T)\cdot C(T)$ product was calculated by equation (5)

$$\gamma_{HS}(T)\ C(T) = \left(\delta_{obs} - \delta_{dia/LS}\right)T = y(T) \tag{5}$$

The plot of $y(T)$ over $\frac{1}{T}$ can be fitted to the sigmoidal function (6) (growth/sigmoidal – Boltzmann included in Origin package)

$$y(x) = \frac{A_1 - A_2}{1 + e^{(x - x_0)/dx}} \tag{6}$$

Using $x = \frac{1}{T},\ x_o = \frac{1}{T_{1/2}} = \frac{\Delta S}{\Delta H},\ dx = \frac{R}{\Delta H}, A_2 = 0$ (for a perfect fit) and $A_1 = C^0$.

A summary of the results is given in Table 3-SI and Table 4-SI. Figures 5-SI and 7-SI give the fitting results for the dmf solution as an example.

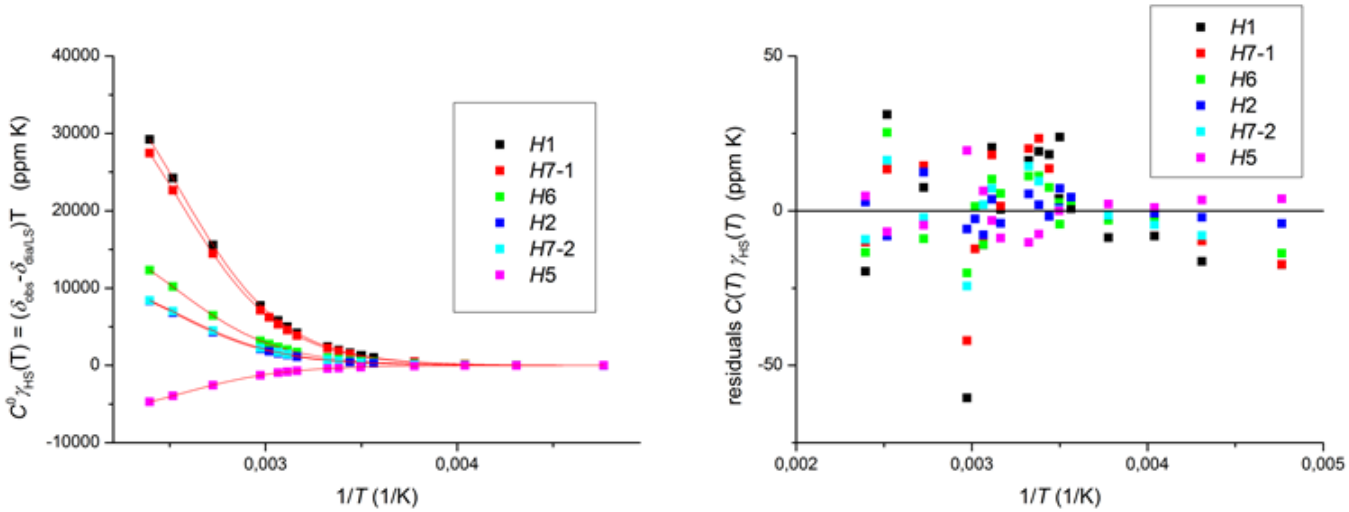

Figure 5-SI left) Plot of the fitting results for [Fe(*rac-trans*-**5**)]$^{2+}$ in d_7-dmf solution. The coloured squares give the experimentally obtained points and the red line represents the best fit by using a sigmoidal curve according to (6). For numerical results see Table 3-SI and Table 4-SI, note that this fitting is with individual $\Delta_{SCO}H$ and $\Delta_{SCO}S$ for every proton site; right) residuals for the fitting.

Table 3-SI: Summary for classical fitting of experimental proton chemical shifts to theoretical calculated shifts (equation (6) using a classical model with constant Curie constant C^0 for complex [Fe(*rac-trans*-**5**)]$^{2+}$ in d_5-pyridine, d_5-nitrobenzene and d_7-dmf. The standard error is given in parentheses as obtained from the fit using Origin program package. The upper and lower confidence limits can be calculated using Student's function.

Proton/solvent	A_2 (ppm K)	A_1 (ppm K)	x_0 (K^{-1})	dx (K^{-1})	Adj.-R^2	Data points (n)/ Degree of Freedom (=n-p)
*H*1 / d_5-pyridine	49950(1607)	-13(34)	262(2)·10^{-5}	277(3.5) 10^{-6}	0,99994	16/12
*H*1 / d_5-nitrobenzene	44774(123)	24(52)	283(0.2)·10^{-5}	292(1.4) 10^{-6}	0,99999	22/18
*H*1 / d_7-dmf	45739(249)	-4(13)	255(0.3)·10^{-5}	269(1.0) 10^{-6}	0,99999	17/13
Average for *H*1	46821					
*H*7-1 / d_5-pyridine	42073(1499)	183(45)	265(1.6) 10^{-5}	265(4.3) 10^{-6}	0,99993	13/9
*H*7-1 / d_5-nitrobenzene	40843(95)	227(37)	281(0.12) 10^{-5}	296(1.2) 10^{-6}	0,99999	22/18
*H*7-1 / d_7-dmf	43612(214)	0,8(10,7)	254(0.3) 10^{-5}	268(0.9) 10^{-6}	0,99999	15/11
Average for *H7-1*	42176					
H6 / d_5-pyridine	21190(633)	-11(12)	261(1.4) 10^{-5}	274(3.1) 10^{-6}	0,99995	16/12
H6 / d_5-nitrobenzene	19357(50)	-6(19)	280(0.1) 10^{-5}	296(1.3) 10^{-6}	0,99999	22/18
H6 / d_7-dmf	19618(140)	5(7)	254(0.4) 10^{-5}	267(1.3) 10^{-6}	0,99999	17/13
Average for *H6*	20055					
H2 / d_5-pyridine	14166(544)	-54(10)	261(1.8) 10^{-5}	271(3.9) 10^{-6}	0,99992	16/12
H2 / d_5-nitrobenzene	13501(33)	-14(13)	280(0.1) 10^{-5}	296(1.2) 10^{-6}	1	19/15
H2 / d_7-dmf	13501(67)	-1(3)	252(0.3) 10^{-5}	267(0.9) 10^{-6}	0,99999	18/14
Average for *H2*	13723					
NH / d_5-pyridine	10825(3056)	-18(20)	233(13.8) 10^{-5}	325(18.4) 10^{-6}	0,99948	
NH / d_5-nitrobenzene	6279(171)	-244(90)	277(1.1) 10^{-5}	323(15.7) 10^{-6}	0,99987	
NH / d_7-dmf	5409(79)	3(3)	251(0.8) 10^{-5}	252(2.4) 10^{-6}	0,99996	
Average for *NH*	7505					
*H*7-2 / d_5-pyridine	13753(497)	71(11)	263(1.7) 10^{-5}	277(4.0) 10^{-6}	0,99992	16/12
*H*7-2 / d_5-nitrobenzene	12530(59)	113(25)	283(2.4) 10^{-5}	298(2.5) 10^{-6}	0,99998	21/17
*H*7-2 / d_7-dmf	13148(143)	-1(8)	255(6.2) 10^{-5}	270(2.2) 10^{-6}	0,99998	12/8
Average for *H7-1*	13143					
H5 / d_5-pyridine	-8134(349)	-110(8.4)	264(2.1) 10^{-5}	274(0.5) 10^{-6}	0,9999	13/9
H5 / d_5-nitrobenzene	-7701(136)	-39(68)	284(0.8) 10^{-5}	296(1.1) 10^{-6}	0,99983	12/8
H5 / d_7-dmf	-7311(88)	3(5)	256(0.7) 10^{-5}	269(0.2) 10^{-6}	0,99997	14/10
Average for *H5*	-7716					

Table 4-SI: Thermodynamic parameters $\Delta_{SCO}H$, $\Delta_{SCO}S$, $T_{1/2}$ calculated from data given in Table 3. The symmetric confidence limit for 99.7% confidence is given in parenthesis. For example with 99.7% confidence (equivalent to 3 σ) $T_{1/2}$ of complex [Fe(*rac-trans*-**5**)]$^{2+}$ in d_5-pyridine is between (381.7 K-4.2 K) and (381.7 K+4.2 K).

Proton/solvent	$T_{1/2}$ (K)	ΔH (kJ/mol)	ΔS $(J/mol \cdot K)$
*H*1/d_5-pyridine	381.7(±4.2)	30.0(±0.4)	78.6(±4.1)
*H*1/d_5-nitrobenzene	353.4(±0.3)	28.5(±0.1)	80.6(±1.4)
*H*1/d_7-dmf	392.2(±0.9)	30.9(±0.1)	78.9(±1.2)
*H*7-1/d_5-pyridine	377.4(±4.8)	31.3(±0.7)	83.1(±5.8)
*H*7-1/d_5-nitrobenzene	355.9(±0.3)	28.1(±0.2)	78.8(±1.1)
*H*7-1/d_7-dmf	393.7(±0.8)	30.9(±0.2)	78.7(±1.1)
H6 / d_5-pyridine	383.1(±3.9)	30.3(±0.6)	79.0(±3.7)
H6 / d_5-nitrobenzene	357.1(±0.3)	28.0(±0.2)	78.5(±1.2)
H6 / d_7-dmf	393.7(±1.1)	31.1(±0.3)	79.1(±1.5)
H2 / d_5-pyridine	383.1(±4.9)	30.6(±0.8)	80.0(±4.8)
H2 / d_5-nitrobenzene	357.1(±0.3)	28.0(±0.2)	78.5(±1.2)
H2 / d_7-dmf	396.8(±0.8)	31.0(±0.2)	78.2(±1.0)
NH / d_5-pyridine	429.2	25.6	59.5
NH / d_5-nitrobenzene	361.0	25.8	71.3
NH / d_7-dmf	398.4	33.0	82.9
*H*7-2 / d_5-pyridine	380.2(±4.7)	30.0(±0.8)	78.9(±4.8)
*H*7-2 / d_5-nitrobenzene	353.4(±0.5)	27.9(±0.4)	79.0(±2.3)
*H*7-2 / d_7-dmf	392.2(±2.0)	30.7(±0.5)	78.5(±2.8)
H5 / d_5-pyridine	378.8(±6.1)	30.3(±1.1)	80.0(±6.4)
H5 / d_5-nitrobenzene	352.1(±2.1)	28.1(±2.1)	79.7(±12.1)
H5 / d_7-dmf	390.6(±2.1)	30.9(±0.5)	79.1(±2.8)
*Avarage** / d_5-pyridine	381	30.4	80.0
*Avarage** / d_5-nitrobenzene	355	28.1	79.2
*Avarage** / d_7-dmf	393	30.9	78.7

* all protons in the table, with the exception of the N*H* proton

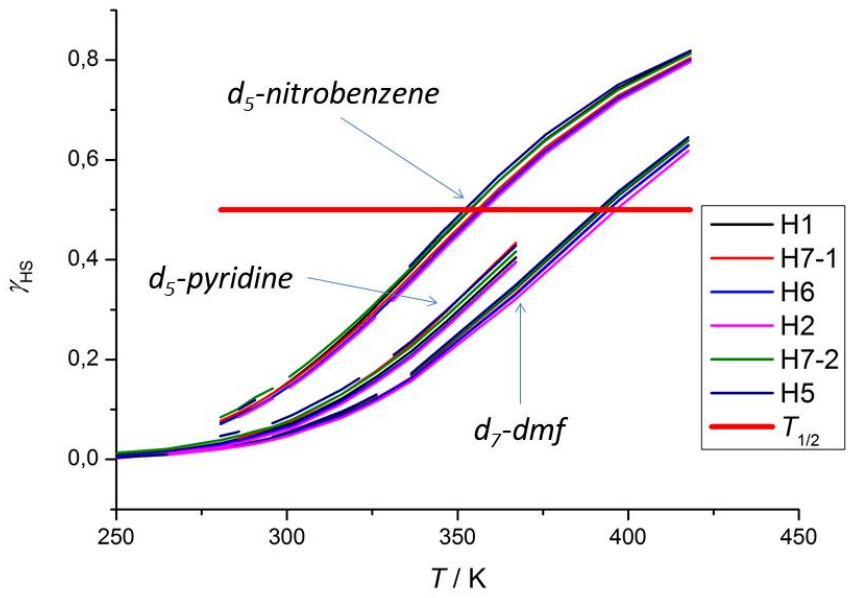

Figure 6-SI: Calculated HS fraction of complex [Fe(*rac-trans-***5**)]$^{2+}$. The curves were obtained by classical fit of the observed chemical shifts for a particular proton on a Boltzmann equation (6). In this classical fit, the Curie constant was treated as temperature independent $C(T) = C^0$. The estimated chemical shifts for the LS species used in these calculations, as well as the obtained thermodynamic parameters are given in Table 4. The red line named $T_{1/2}$ is drawn at γ_{HS} = 0.5 as a guide for the eyes, crossings of this line with the calculated curves define $T_{1/2}$.

1.4.6 Improved Refinement with First Order Correction of C(T) using $C^1 \neq 0$

Using a classical refinement as described in 1.4.5, leads to different results for $\Delta_{SCO}H$ and $\Delta_{SCO}S$ depending on the proton site used. The differences mainly arise from the temperature dependence of Curie constants for a particular proton C_i(T). Using a linearly corrected $C_i(T) = C_i{}^0 + C_i{}^1 T$ with individual C^0 and C^1 for a particular proton position, it is possible to describe the experimental chemical shifts with one global $\Delta_{SCO}H$ and $\Delta_{SCO}S$. For reasons which are outlined below, we used the averaged thermodynamic $\Delta_{SCO}S$ and $\Delta_{SCO}H$ values obtained from classical treatment

(Table 4). These values ($\Delta_{SCO}H$ and $\Delta_{SCO}S$) were fixed for the refinement. The diamagnetic contributions $\delta_{dia/LS}$ and C^0 and C^1 for a particular proton and for all solvents were refined independently. The least squares refinement was done with a homemade Excel-script. The square of the difference between calculated and observed chemical shifts were used to directly monitor the progress. Weighting schemes were not applied. As can be seen from Figure 7 and Figure 8, the introduction of C^1 as a linear correction term significantly improves the coherence of the calculated HS fractions that derive from different proton sites ($\gamma_{HS} \ll 0.5\%$; equation (7) with fitted C^0,C^1, $\delta_{dia/LS}$), meaning that the experimentally observed chemical shift can be reproduced very well ($\Delta\delta < 0.2\ ppm$ (Figure 8)). In fact, this equals the achievable accuracy of NMR experiments. The drawback of this approach is that the application of C^1 as a linear correction is very efficiently masking experimental problems, if present. Therefore agreement between experimental data and calculated data can be observed for larger ranges of $\Delta_{SCO}H$ / $\Delta_{SCO}S$ / C_i^1 triples indicating over-parameterization. Over-parameterization can be avoided by fixing one parameter; in case of the classical refinement all C_i^1 are fixed to zero. Fixing C^1 to zero will lead automatically to a systematic error in $\Delta_{SCO}H$ / $\Delta_{SCO}S$. This error is usually small because C^1 is small; at least for rigid Fe^{2+} complexes, for reasons outlined in section 1.4.4.1. It is recommended to set C^1 to zero and apply fixed and reasonable values for $\delta_{dia/LS}$, especially when NMR spectra can be recorded only in a small temperature range and no data points significantly higher than $T_{1/2}$ are available. The NMR data used in these calculations (results for Figure 7-SI and Figure 8-SI) was measured in a comparably large range (> 200 K) from 210 K to 418 K and excellent agreement was observed for all protons including the amine proton (N*H*).

$$\gamma_{HS}(T) = \frac{(\delta_{obs} - \delta_{dia/LS})T}{(C^0 + C^1 T)} \tag{7}$$

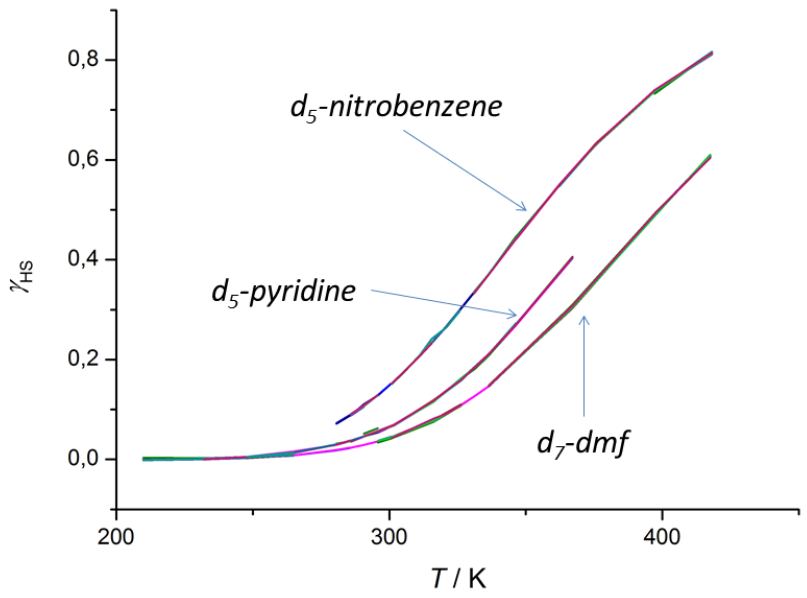

Figure 7-SI: Calculated HS fraction for complex [Fe(*rac-trans*-**5**)] using proton chemical shifts and parameters C^0,C^1, $\delta_{dia/LS}$ (individually refined for each proton with global $\Delta_{SCO}H$ and $\Delta_{SCO}S$ taken from classical refinement Table 4 (averaged values)). The same proton sites have been used as previously in Figure 6-SI.

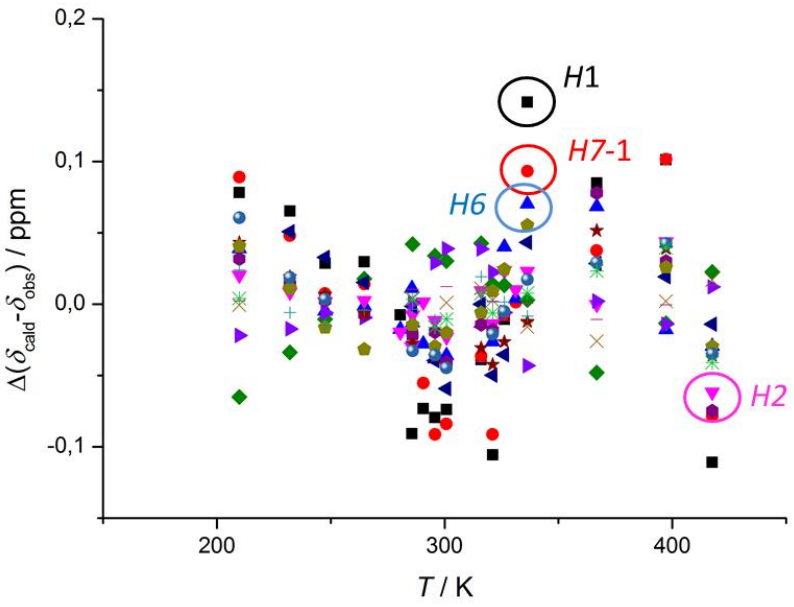

Figure 8-SI: Difference between calculated (with best fit parameters C^0, C^1, $\delta_{dia/LS}$ (equation (**7**))) and observed chemicals shifts for complex [Fe(*rac-trans*-**5**)]$^{2+}$ in d_7-dmf solution for all protons. Averaged values from classical refinement $\Delta_{SCO}H$ = 30.9 kJ / mol and $\Delta_{SCO}S$ = 78.7 J/(mol K) were used to calculate the high spin fraction $\boldsymbol{\gamma_{HS}(T)}$ (equation (**3**)) (see Table 4-SI).

1.4.7 Fitting of Data with Limited Temperature Range – Parameterised Refinement

In order to obtain thermodynamic parameters for complex [Fe(*rac-trans*-**5**)]$^{2+}$ in acn, dmso and D_2O, the HS fractions were calculated by using the diamagnetic shifts $\delta_{dia/LS}$ extracted from the NMR data in d_7-dmf-solutions and the average values of C^0 obtained from classical fit in d_5-pyridine, d_7-DMF and d_5-nitrobenzene solutions (Table 3-SI). The calculated HS fractions (equation (7) with C^1 = 0) were used again for fitting against a Boltzmann distribution equation (3 and (10). Similar to the calculations above, only the six protons *H*1, *H*7-1, *H*6, *H*2, *H*7-2, *H*5 were used for the calculations.

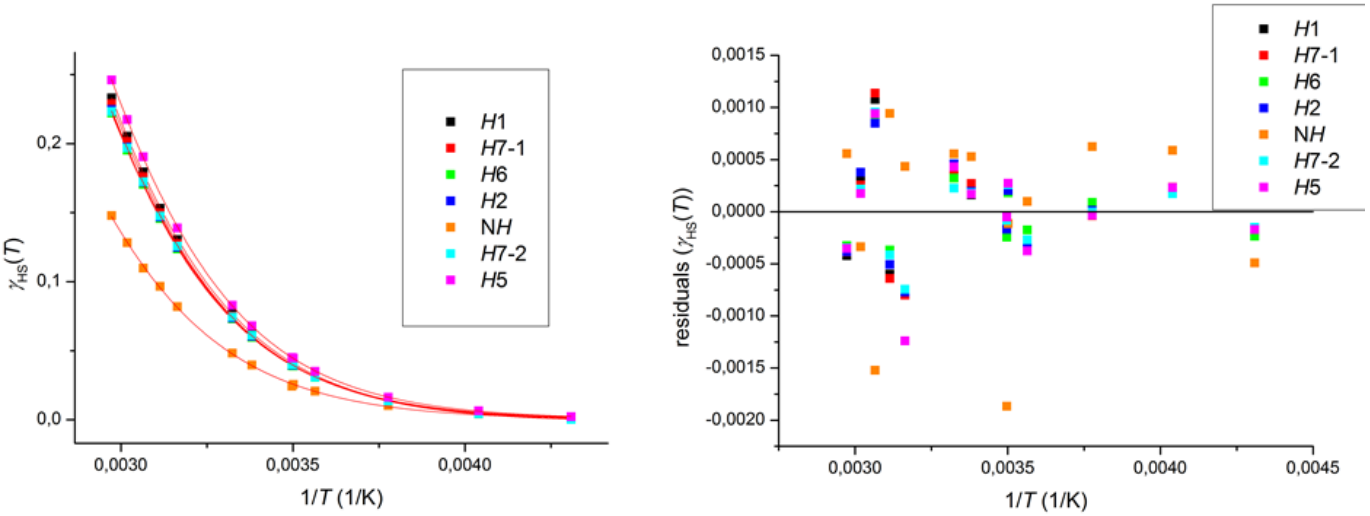

Figure 9-SI left) Plot of the fitting results for [Fe(*rac-trans*-**5**)]$^{2+}$ in d_3-acn solution. The colored squares give the experimentally obtained points and the red lines represents the best fit by using a sigmoidal curve according to (7) with C^1 fixed to zero and C^0 fixed at values taken from solution studies in d_7-dmf, d_5-nitrobenzene and d_5-pyridine (Table 3). For numerical results see Table 3 and Table 4, note that this fitting is with individual $\Delta_{SCO}H$ and $\Delta_{SCO}S$ for every proton site; right) Residuals for the fitting are shown. The N*H* proton was included to demonstrate, that using NMR data from limited temperature range can give excellent fits but wrong results. The use of a "many proton sites" approach helps to minimise the error.

Table 5-SI: Summary for fitting $T_{½}$, $\Delta_{SCO}H$ and calculated $\Delta_{SCO}S$ for complex [Fe(*rac-trans*-**5**)]$^{2+}$ in acn solution. Temperature range was from 232 K to 336 K.

Proton/ACN	x_0 (K^{-1})	dx (K^{-1})	Adj.-R^2	n / n-p	$T_{1/2}$ (K)	ΔH (kJ/mol)	ΔS $(J/mol \cdot K)$
*H*1	266(0.21) 10^{-5}	268(1.3) 10^{-6}	0.99989	13/11	375.9(0.3)	31.0(0.15)	82.4
*H*7-1	265(0.22) 10^{-5}	267(1.3) 10^{-6}	0.99989	13/11	377.4(0.3)	31.1(0.15)	82.5
*H*6	264(0.16) 10^{-5}	270(1.0) 10^{-6}	0.99994	13/11	378.8(0.2)	30.8(0.1)	81.3
*H*2	264(0.14) 10^{-5}	270(0.8) 10^{-6}	0.99996	13/11	378.8(0.2)	30.8(0.1)	81.4
*H*7-2	264(0.31) 10^{-5}	272(1.8) 10^{-6}	0.99979	13/11	378.8(0.5)	30.6(0.2)	80.8
*H*5	267(0.15) 10^{-5}	271(1.0) 10^{-6}	0.99994	12/10	374.5(0.2)	30.7(0.1)	81.9
				Average	377.4	30.8	81.7
				max	378.8	31.1	82.5
				min	374.5	30.6	80.8

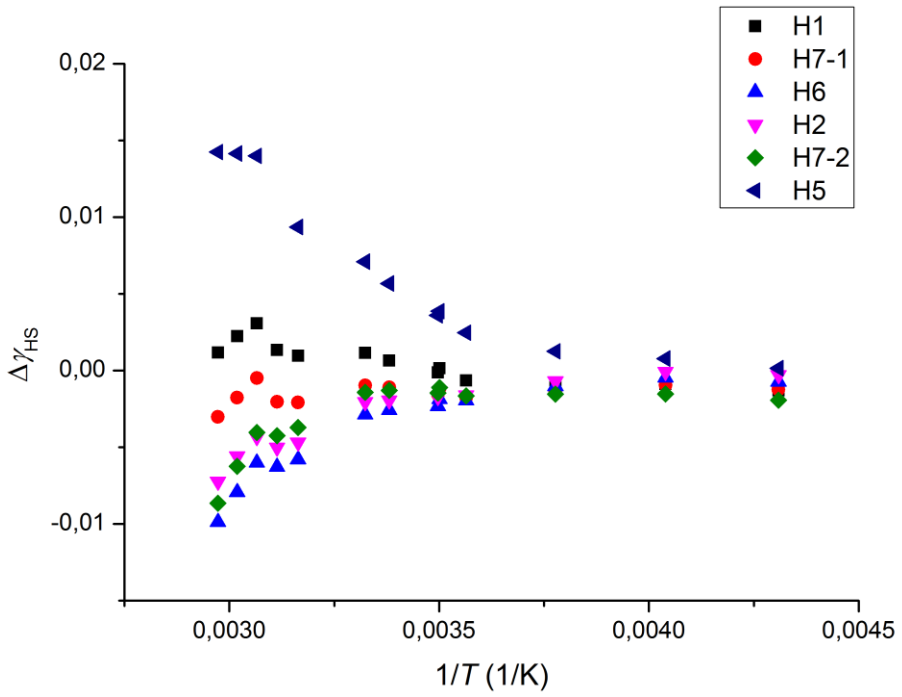

Figure 10-SI: Difference between HS fraction of complex [Fe(*rac-trans*-**5**)]$^{2+}$ in d_3-acn solution calculated from NMR data (with fixed C^0 (see Table 4) and C^1 = 0 and $\delta_{dia/LS}$ values from dmf solution) and calculated from Boltzmann distribution $T_{1/2}$ = 377.4 K, $\Delta_{SCO}H$ = 30.8 kJ/mol and $\Delta_{SCO}S$ = 81.7 J/(mol K).

The fitting results shown in Figure 8 clearly give evidence of an unaccounted temperature dependence. Improved matching is again obtained by using C^1 as correction parameters and free refinement of $\delta_{dia/LS}$. Fitting with homemade excel program allows to obtain excellent agreement (Figure 11) between HS fraction calculated by the NMR data (equations (4) and (5)) and using a Boltzmann distribution (equation (10)).

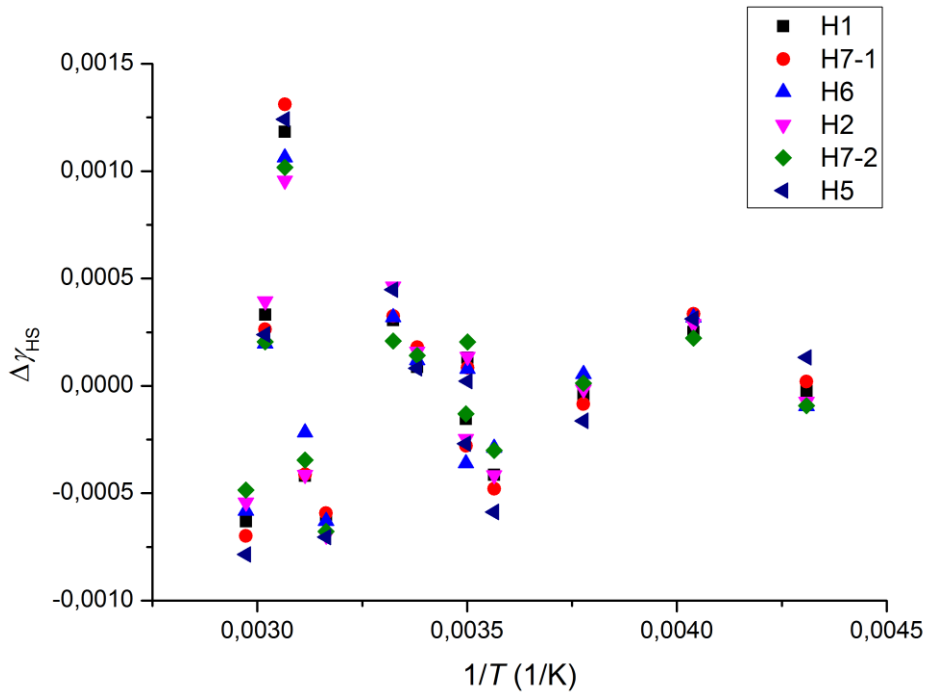

Figure 11-SI: Difference between HS fractions for complex [Fe(*rac-trans*-**5**)]$^{2+}$ in acn solution calculated using the NMR parameters (equation 5) and using Boltzmann distribution(equation 3).

Table 6-SI: Summary of fitted $T_{½}$, $\Delta_{SCO}H$ and calculated $\Delta_{SCO}S$ for complex [Fe(*rac-trans*-**5**)]$^{2+}$ in DMSO solution. Temperature range was between 301 K and 419 K.

Proton/DMSO	x_0(K^{-1})	dx(K^{-1})	Adj.-R^2	n / n-p	$T_{1/2}$ (K)	ΔH (kJ/mol)	ΔS $(J/mol \cdot K)$
*H*1	248(0.82) 10^{-5}	271(0.75) 10^{-6}	0.99996	9/7	403.2(0.13)	30.7(0.9)	76.2
*H*7-1	250(0.75) 10^{-5}	261(0.69) 10^{-6}	0.99997	9/7	400.0(0.12)	31.8(0.8)	79.5
*H*6	247(0.68) 10^{-5}	269(0.62) 10^{-6}	0.99997	9/7	404.9(0.11)	30.9(0.7)	76.2
*H*2	246(0.90) 10^{-5}	270(0.84) 10^{-6}	0.99995	9/7	406.5(0.15)	30.8(1.0)	75.9
*H*7-2	250(0.88) 10^{-5}	262(0.82) 10^{-6}	0.99995	9/7	400.0(0.14)	31.7(1.0)	79.2
*H*5	247(0.76) 10^{-5}	283(0.68) 10^{-6}	0.99997	8/6	404.9(0.13)	29.4(0.7)	72.5
				Average	403.2	30.8	76.6
				max	406.5	31.8	79.5
				min	400.0	29.4	72.5

Table 7-SI: Summary of $T_{½}$, $\Delta_{SCO}H$ and calculated $\Delta_{SCO}S$ for complex [Fe(*rac-trans*-**5**)]$^{2+}$ in D_2O solution. Temperature range was between 280 K and 376 K.

Proton/D_2O	x_0(K^{-1})	dx (K^{-1})	Adj.-R^2	n / n-p	$T_{1/2}$ (K)	ΔH (kJ/mol)	ΔS $(J/mol \cdot K)$
*H*1	247(0.11) 10^{-5}	245(0.6) 10^{-6}	0.99996	12/10	404.9(0.2)	33.9(0.9)	83.9
*H*7-1	245(0.06) 10^{-5}	247(0.4) 10^{-6}	0.99999	12/10	408.2(0.1)	33.7(0.5)	82.5
*H*6	246(0.09) 10^{-5}	247(0.5) 10^{-6}	0.99997	12/10	406.5(0.2)	33.7(0.7)	82.9
*H*2	246(0.07) 10^{-5}	245(0.4) 10^{-6}	0.99998	12/10	406.5(0.1)	33.9(0.6)	83.3
*H*7-2	247(0.17) 10^{-5}	249(1.0) 10^{-6}	0.9999	12/10	404.9(0.3)	33.4(1.3)	82.6
*H*5	246(0.07) 10^{-5}	249(0.4) 10^{-6}	0.99998	11/9	406.5(0.1)	33.4(0.5)	82.1
				Average	406.2	33.7	82.9
				max	408.2	33.9	83.9
				min	401.6	33.4	82.1

1.4.8 Fitting of NMR Data for the methylated Complex [Fe(rac-trans-NMe-5)]$^{2+}$

In order to obtain the transition temperatures $T_{½}$ for the methylated complex [Fe(rac-*trans-NMe*-**5**)]$^{2+}$, the average Curie coefficients obtained for the non-methylated counterparts were used (Table 3-SI). The Curie coefficients C^0 (eq. (4), C^1 is set to zero) were fixed and, with least-square refinement, the diamagnetic shifts $\delta_{dia/LS}$ as well as $\Delta_{SCO}H$ and $\Delta_{SCO}S$ were refined freely by using our Excel script. Only the protons (C^0 in ppm K) *H*1 (46821), *H*2 (13723), *H*5 (-7716), *H*6 (20055) and *H*7-1 (42176) were used (results are compiled in Table 8-SI first line). Additionally, from the individual Curie constants (C^1 = 0) of every proton site, the HS fractions were calculated using $\delta_{dia/LS}$ values from d_7-dmf solution. These HS fractions were used to individually extract $\Delta_{SCO}H$ and $\Delta_{SCO}S$ from a fit to the Boltzmann distribution (10) and (3) for each proton using the Origin program package. The results are summarized in Table 8. The Curie constant of proton *H*7-2 is markedly affected by methylation (13143 ppm K for complex [Fe(*rac-trans*-**5**)]$^{2+}$ and about 8500 ppm K for [Fe(*rac-trans-NMe*-**5**)]$^{2+}$). This finding agrees well with the molecular structure investigated by single crystal x-ray analysis that shows close contact between *H*7-2 and the methyl group (Me ··· H distance < 2.6 Å). Nevertheless, the proton *H*7-2 as well as the rest of the signals follow the Curie law and can be reproduced by free refinement of C^0. Again excellent agreement between experimentally and

calculated chemical shifts can be obtained by using eq. (4) and free refinement of C^1 with fixed global $\Delta_{SCO}H$ and $\Delta_{SCO}S$.

Table 8-SI: Summary of the thermodynamic parameters of the methylated complexes [Fe(*rac-trans-NMe-***5**)]$^{2+}$ in different solvents. (Least-squares refinement using five different proton sites; $T_{½}$ in K, $\Delta_{SCO}H$ in kJ/mol and $\Delta_{SCO}S$ in J/(mol·K). Proton site *H*5 gives unsatisfying results; obviously the coupling between the unpaired electrons and *H*5 is solvent dependent.

Proton \ solvent	acn / acetic acid (2.5 : 4)			d_6-dmso			d_3-acn			d_5-nitrobenzene		
	$T_{1/2}$	$\Delta_{SCO}H$	$\Delta_{SCO}S$	$T_{1/2}$	$\Delta_{SCO}H$	$\Delta_{SCO}S$	$T_{1/2}$	$\Delta_{SCO}H$	$\Delta_{SCO}S$	$T_{1/2}$	$\Delta_{SCO}H$	$\Delta_{SCO}S$
all in one*	433	32.4	74.8	442	32.5	73.6	427	33.9	79.3	432	33.1	76.5
*H*1	429.2 (0.7)	33.0 (0.1)	77.0	440.5 (0.2)	33.0 (0.1)	74.8	425.5 (1.1)	34.0 (0.3)	80.0	431.0 (0.4)	33.6 (0.2)	77.9
*H*7-1	440.5 (0.6)	31.0 (0.1)	70.4	442.5 (0.4)	31.6 (0.2)	71.5	434.8 (0.8)	32.1 (0.2)	73.7	434.8 (0.5)	32.1 (0.2)	73.8
*H*6	440.5 (0.7)	31.0 (0.1)	70.4	442.5 (0.4)	31.9 (0.2)	72.1	436.7 (0.9)	32.0 (0.2)	73.2	434.8 (0.4)	32.5 (0.2)	74.7
*H*2	431.0 (0.6)	32.85 (0.2)	76.2	438.6 (0.1)	33.5 (0.06)	76.3	425.5 (0.9)	34.0 (0.2)	80	429.2 (0.3)	34.2 (0.2)	79.7
*H*5	406.5 (2.2)	39.4 (0.8)	96.9	433.0 (1.7)	35.9 (1.3)	82.9	406.5 (3.8)	39.2 (0.2)	96.3	404.9 (7)	40.9 (3.2)	101.1

* least squares refinement using all five proton sites

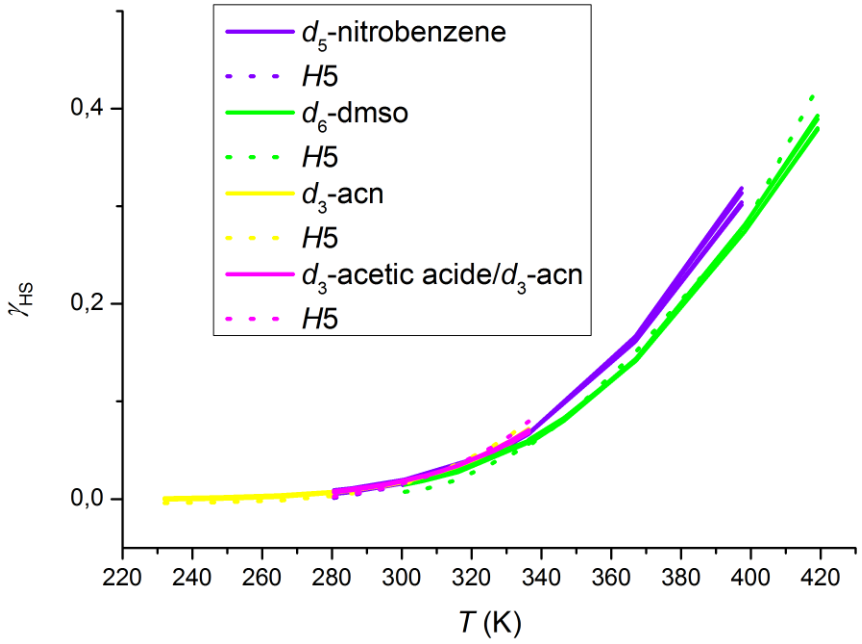

Figure 12-SI: Temperature dependence of the calculated HS–fraction γ_{HS} for the methylated complex [Fe(*rac-trans-NMe-***5**)]$^{2+}$. The calculation is based on equation (7) and fixed C^0 (Table 3-SI). The correction parameter C^1 was set to zero.

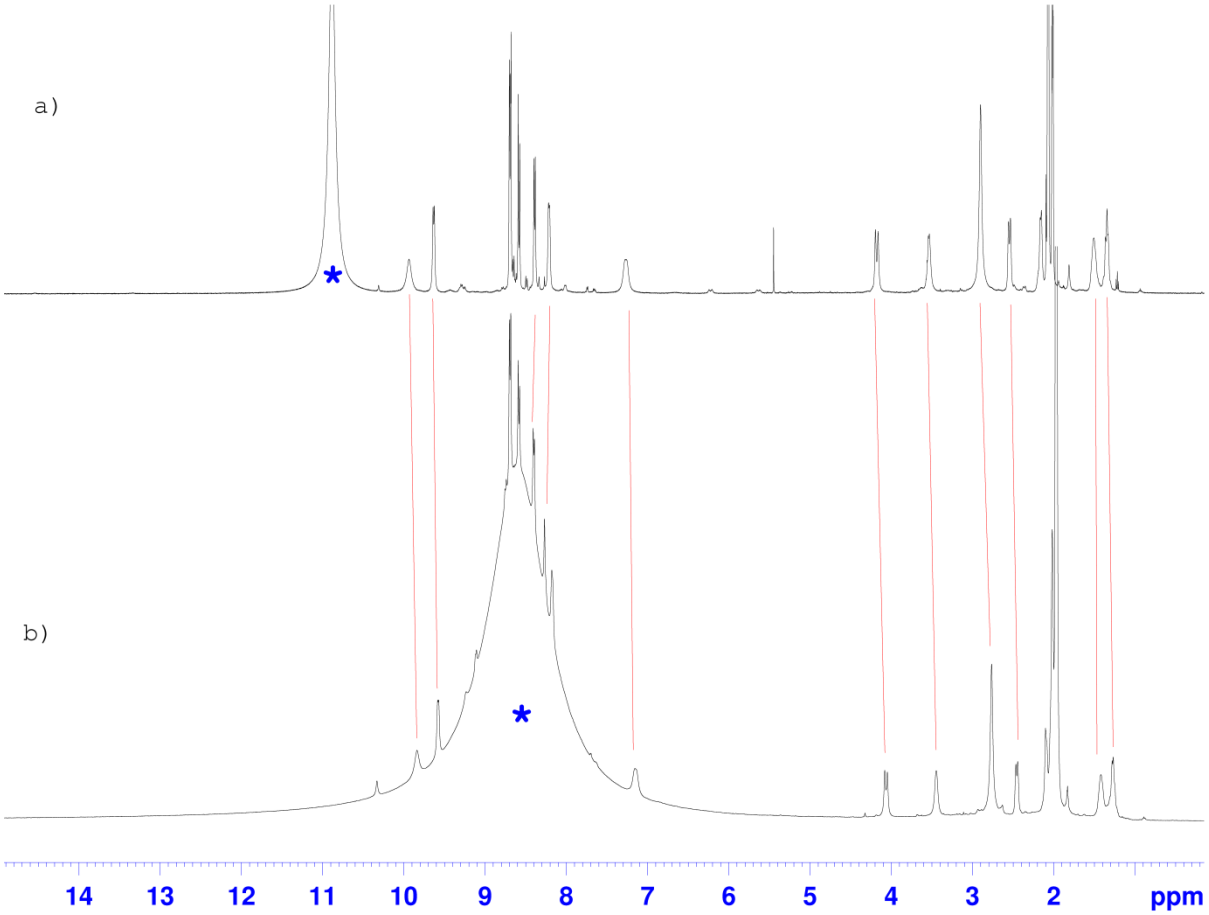

Figure 13-SI: a) ^{1}H NMR spectrum of complex [Fe(*rac-trans-NMe-***5**)]$^{2+}$ in acetic acide/acn 2.5 : 4 and b) the same sample after a year standing in solution on the bench without any preclusions of air or moisture. The star * mark the water/AcO*H* peak that increased due to the absorption of moisture.

1.4.9 Fitting of NMR Data for [Fe(6)]$^{2+}$ with high $T_{1/2}$

Using Curie constants C^0 for identical proton sites of the same or similar complexes, $T_{½}$, $\Delta_{SCO}H$ and $\Delta_{SCO}S$ can be extracted from NMR data with limited temperature range below $T_{½}$. This was outlined in 1.4.8 for complex [Fe(*rac-trans-NMe-***5**)]$^{2+}$; for example, data from acn/acetic acid was used with maximum HS-fraction less than 10%. For

[Fe(*rac-trans-NMe*-**6**)]$^{2+}$, the maximum HS-faction is less than 3%. This problem can be tackled by further reducing the number of parameters to be refined.

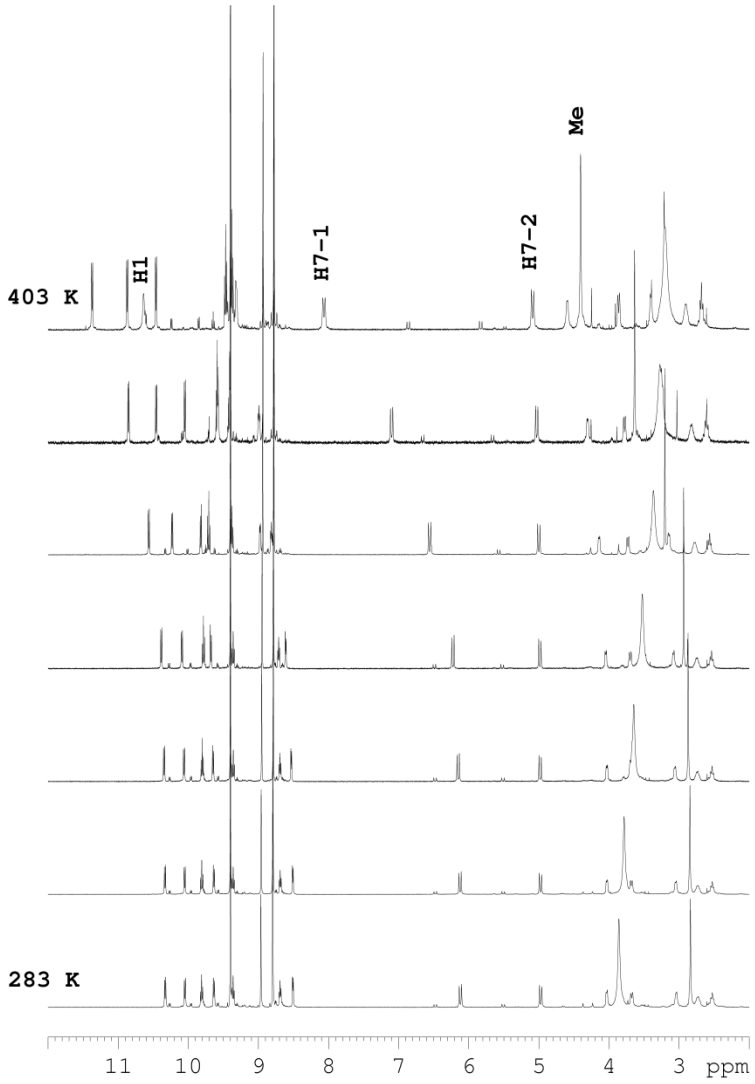

Figure 14-SI: VT-NMR spectra of [Fe(*rac-trans-NMe*-**6**)]$(BF_4)_2$ in d_5-nitrobenzene.

In order to obtain an estimate for $T_{1/2}$ of complex [Fe(*rac-trans-NMe*-**6**)]$^{2+}$, the obtained chemical shifts for the protons were fitted by using the averaged C^0 values (Table 4-SI). These values were obtained from the classical treatment of complex [Fe(*rac-trans*-**5**)]$^{2+}$ (C^1 = 0). The C^0-values for particular proton sites were chosen by structural similarity. With a view on the structural similarity, the assumption of similar C^0 values of *H*1, *H*2, *H*5 and both *H*7 for [Fe(*rac-trans*-**5**)]$^{2+}$ and [Fe(*rac-trans-NMe*-**6**)]$^{2+}$ appears reasonable. The protons *H*6 and *H*4' could not be assigned

unambiguously. Protons *H*6 and *H*4' are both in *meta*-position to the nitrogen of the inner pyridine ring so that it appears reasonable to use the C^0 value of *H*6 of complex [Fe(*rac-trans*-**5**)]$^{2+}$ for both protons. The proton *H*4 is akin to *H*2 in *meta*-position to the nitrogen in the terminating pyridine ring and received the same C^0 value as *H*2 in [Fe(*rac-trans*-**5**)]$^{2+}$. The proton *H*3 as well as all protons on the cyclohexyl fragment and the methyl protons were not used. The correction parameter C^1 was set to zero in all cases and the diamagnetic contribution $\delta_{dia/LS}$ is well defined in spectra recorded below room temperature and was refined freely. As shown above, the entropy change $\Delta_{SCO}S$ for the SCO falls in a narrow range at approximately 80 J/mol K. Hence, the value for $\Delta_{SCO}S$ was fixed to 80 J/mol K. Fixing $\Delta_{SCO}S$ reduces the number of parameters and allows a stable refinement. The enthalpy change $\Delta_{SCO}H$ is the only parameter to be refined. This parameter $\Delta_{SCO}H$ was varied to obtain good agreement between experimental and calculated values; this was the case for $\Delta_{SCO}H$ = 45.5 kJ/mol K. The transition temperature $T_{1/2}$ is therefore calculated as 570 K. In the light of the assumptions made and rather small HS-fraction in this temperature range this can be only a rough estimate with large uncertainty of about ±30-50 K. The agreement of the experimentally obtained and the calculated shifts (Figure 15) is fairly good. The exception noted for *H*7-2 is due to the close contact to the methyl group (Me ··· H distance 2.48 Å).

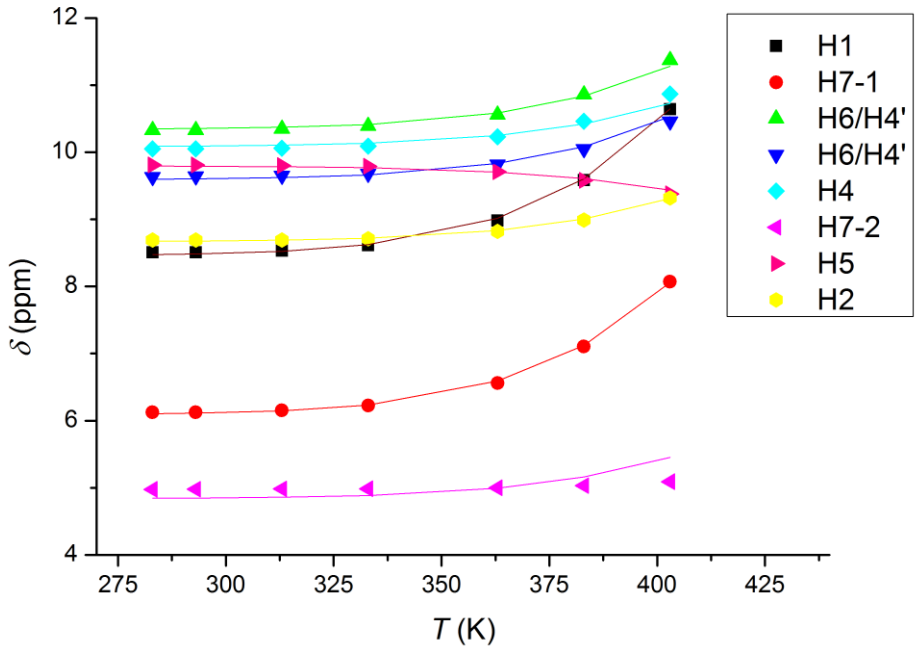

Figure 15-SI: Calculated (lines) and experimentally obtained chemical shifts for [Fe(*rac-trans-NMe-***6**)]$^{2+}$

1.5 Temperature Dependent UV/Vis Spectroscopy

Temperature dependent UV/Vis spectroscopy was used as a second independent source of thermodynamic parameters, in order to validate the NMR-derived data. It turned out that the coherence between both methods strongly depends on the applied processing procedure. Several experimental obstacles need to be addressed. Therefore methods that finally lead to a good agreement are described in details below.

1.5.1 Solution Samples

Temperature dependent UV/Vis spectra were recorded using a homemade sample holder. This holder employs a flat UV/vis cuvette with 1 mm cell thickness. The cuvette is completely surrounded by a housing of aluminum; the

housing has drills to place endings of optical fibres next to the windows of the cuvette in 180° geometry. A warm white power LED (LUXEON K2 LXK2-PWW4-U00, warm white) was used as a light source. The temperature of the housing was controlled by cryogenic controller CTC100 and heated by resistive heating elements. The sample holder was placed in a Dewar vessel and liquid nitrogen was added in order to cool it below ambient temperature. Heating and cooling rates were set to 0.01 K/s.

The optimum concentration of sample was tested in pre-experiments and was chosen to meet the optimum light intensity on the CCD of the spectrometer (≈ 1 mM). The intensity of the transmitted light at 564 nm (I_{564}) was used for subsequent calculations. Our home made sample holder needs to be dismantled each time the cuvette is changed from blank solution to sample solution. These manipulations lead to serious artificial variations in light intensities. For this reason, an accurate determination of the absorbance is not possible. However, the ratio between the light intensities at different wavelengths remains unchanged as long as the same light source is used. In addition, the intensities of the light going through the sample holder are also affected by the expansion of the sample housing with changing temperature. In order to correct fluctuations in the transmitted light, the intensity at 711 nm (I_{711}) was used as internal reference. At 711 nm the absorbance of the LS and HS state is negligible.

The logarithm of corrected light intensity was calculated equivalent to an absorbance A as A_{eq} using equation (8). In contrast to the absorbance, A_{eq} decreases with increasing transmitted light intensity and it has an offset A^0. With the assumption of zero absorbance at 564nm and 711nm of the solvent and the HS complex, the offset is a function of the light source that was used and can be calculated from the light intensities I_{564} and I_{711} measured with a blank solution. For the used light source A^0 is about 0.95 (*vide infra*).

$$A_{eq} = \log 10 \frac{I_{564}}{I_{711}} \tag{8}$$

In order to calculate the HS fraction, the limiting absorbance $A_{eq/HS}$ and $A_{eq/LS}$ for the pure LS and HS state must be estimated (in other words, the molar absorption coefficients ε_i for both species must be set to reasonable values). The respective equivalent absorption $A_{eq/HS}$ for the HS complex was calculated from the reference spectrum of pure solvent with the assumption that the HS complex does neither absorb at 564 nm nor 711 nm. This assumption is based on the observation that all compounds containing [Fe(**5**)]$^{2+}$ turn reversibly to pale red if heated in propylene carbonate to about 500 K. It is a typical observation for similar complexes, that the intense MLCT absorption bands around 580 nm are only found in the LS spin state.[13–16] With this assumption, $A_{eq/HS}$ is equivalent to A^0 (0.95).

The difference $A_{eq}{}' = A_{eq/HS} - A_{eq}$ is now proportional to the concentration of the LS species, provided that the total volume of the solution is conserved. As this is evidently not the case, due to thermally driven expansion and contraction, $A_{eq}{}'$ was corrected for changes in solvent density making use of tabulated functions.[17] With the calculated density the relative density with respect to 290 K was calculated by $\rho_r(T) = \rho(T)/\rho(290\ K)$. The calculated $\rho_r(T)$ was used to correct $A_{eq}{}'$ to obtain $A_{eq}{}'' = {A_{eq}{}'}/{\rho_r(T)}$. As a function describing the density for dmf was not available, the relative density $\rho_r(T)$ calculated for nitrobenzene was also used to approximate the density variation of dmf. With the assumption of negligible absorption of the HS species at 711 nm and 564 nm $A_{eq/HS}$ is not affected by the solvent density. The lower border for the refinement and $A_{eq/LS}{}'$ were set manually to reasonable values. For the nitrobenzene sample, NMR calculated HS fractions at 290 K were used to approximate $A_{eq/LS}{}'$. In case of the acetone and dmf samples, the HS faction at the lowest accessible temperature was small enough to allow reasonable estimates of $A_{eq/LS}{}'$. The HS fraction γ_{HS} was calculated using equation (9).

$$\gamma_{HS}(T) = 1 - \frac{A_{eq}{}''(T)}{A_{eq/LS}{}'} \qquad (9)$$

Similar to the NMR data processing the calculated HS fraction was fitted to a Boltzmann distribution

$$y_{HS}(x) = \frac{1}{1 + e^{(x-x_0)/dx}} \quad (10)$$

by using $x = \frac{1}{T}, x_o = \frac{1}{T_{1/2}} = \frac{\Delta S}{\Delta H}, dx = \frac{\Delta H}{R}$

Plots of the calculated HS fractions and of the fit functions are given in Figure 16-SI to Figure 18-SI and thermodynamic parameters derived from best fit parameters are compiled in Table 9-SI.

1.5.2 Temperature Dependent UV/Vis Spectroscopy on Complexes Embedded in Epoxy Resin.

These samples (for preparation see 1.1.3) were placed in the sample holder with the slide and the lid. Similarly to the solution samples, two ends of an illuminating and receiving fibre were placed close to the sample in 180° geometry. The temperature dependent UV/Vis spectra were recorded and processed similar to the solution samples. At variance to the solution samples, no corrections for expansion of the resin were made. The limiting absorptions $A_{eq/LS}{}'$ were estimated from low temperature data. For A^0 again the limiting absorption $A_{eq/HS}{}'$ was set to 0.95. Plots of the calculated HS fractions and of the fit functions are given in Figure 19-SI to Figure 20-SI and thermodynamic parameters derived from best fit parameters are compiled in Table 9-SI.

Table 9-SI: Results obtained from the temperature dependent UV/vis spectroscopy. The standard error is given behind the value in parentheses as obtained from the fit. The upper and lower confidence limits can be calculated using Student's function (n = number of points, n-p = degree of freedom). For details on the data processing see text above.

Solvent/Complex	$T_{1/2}$ (K)	$\Delta_{SCO}H$ (kJ/mol)	$\Delta_{SCO}S$ $(J/mol \cdot K)$	**n / n-p**
dmf / [Fe(*rac-trans*-**5**)]$^{2+}$	390.6(0.2)	33.4(0.1)	85.5	58/56
nitrobenzene / [Fe(*rac-trans*-**5**)]$^{2+}$	358.4(0.2)	28.1(0.2)	78.3	51/49
acetone/[Fe(*cis*-**5**)]$^{2+}$	276.2(0.1)	20.1(0.1)	72.7	96/94

epoxy resin/[Fe(*rac-trans*-**5**)]$^{2+}$	380.2(0.2)	30.2(0.2)	79.4	79/77
epoxy resin/[Fe(*rac-trans-NMe*-**5**)]$^{2+}$	411.4(0.5)	25.8(0.2)	62.9	163/161

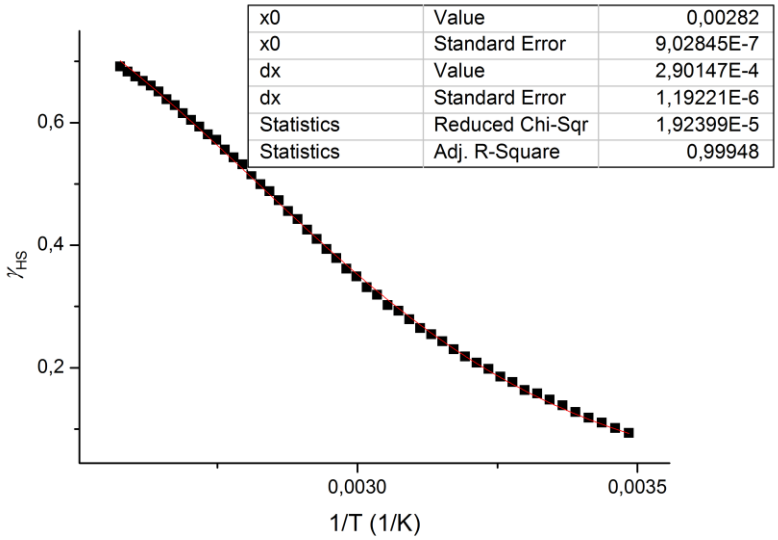

Figure 16-SI: Calculated HS-fraction (black squares) and best fit function (red line) for complex [Fe(*rac-trans*-**5**)]$^{2+}$ in nitrobenzene solution.

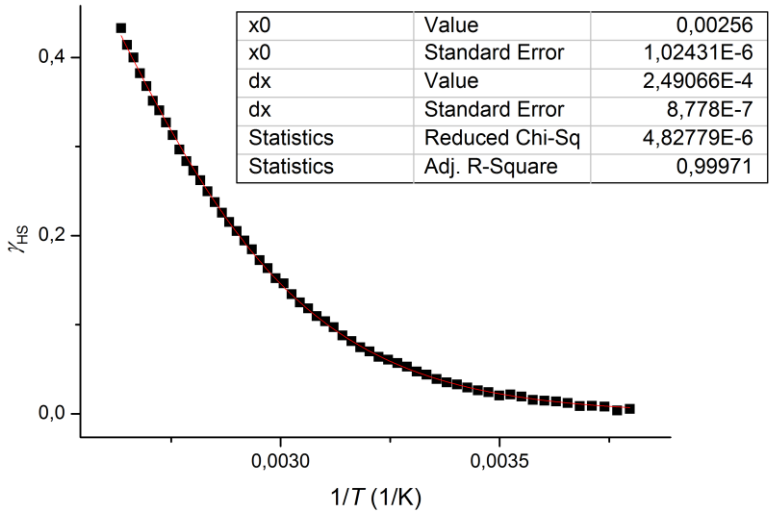

Figure 17-SI: Calculated HS-fraction (black squares) and best fit function (red line) for complex [Fe(*rac-trans*-**5**)]$^{2+}$ in DMF solution.

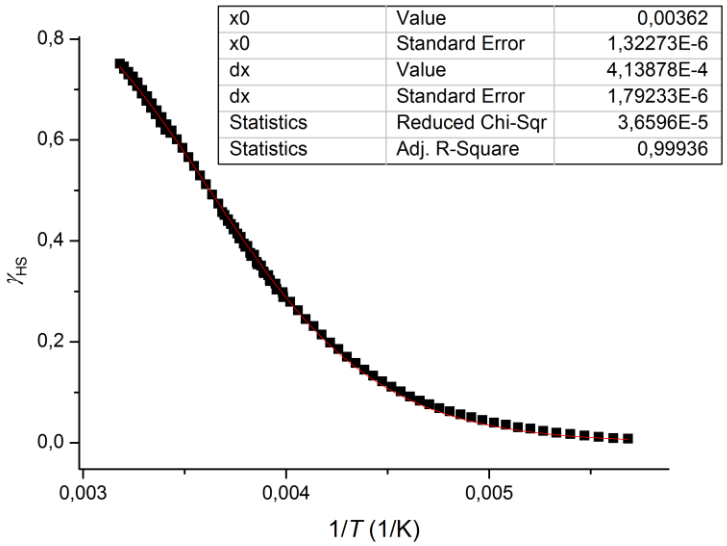

Figure 18-SI: Calculated HS-fraction (black squares) and best fit function (red line) for complex [Fe(*cis*-**5**)]$^{2+}$ in acetone solution.

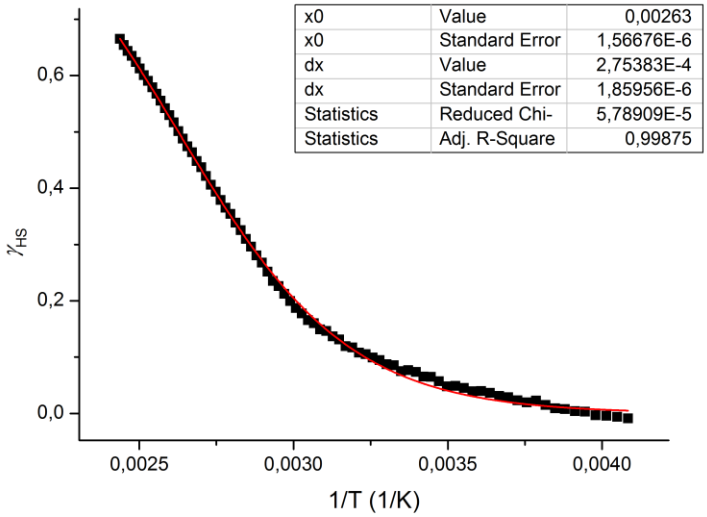

Figure 19-SI: Calculated HS-fraction (black squares) and best fit function (red line) for complex [Fe(*rac-trans*-**5**)]$^{2+}$ embedded into epoxy resin.

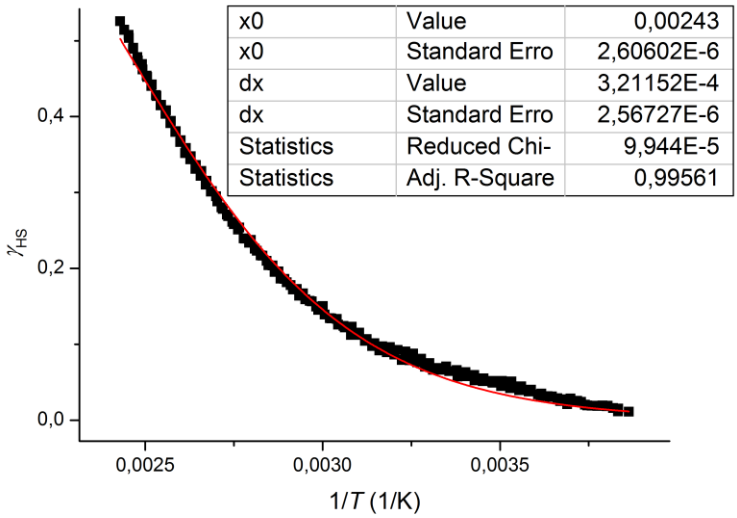

Figure 20-SI: Calculated HS-fraction (black squares) and best fit function (red line) for complex [Fe(*rac-trans-NMe*-**5**)]$^{2+}$ embedded into epoxy resin.

1.6 Relaxation Time Measurements

Relaxation times were measured in d_3-acn solution by the inversion recovery method. Data recording and processing was done with the Bruker Top Spin 2.1 program package. For the inversion recovery experiment, 32 relaxation delays from 0.1ms to 40s were used. The obtained T_1 times are given in Table 10. The obtained T_1 values obey to the $1/r^6$-rule (the intramolecular distances *r* were taken from the X-ray structure analysis of complex [Zn(*rac-trans*-**5**)]$(ClO_4)_2$) and corroborate the assignment of the protons and also allow the unambiguous assignment of *H*7-1 and *H*7-2 (see Table 10-SI).

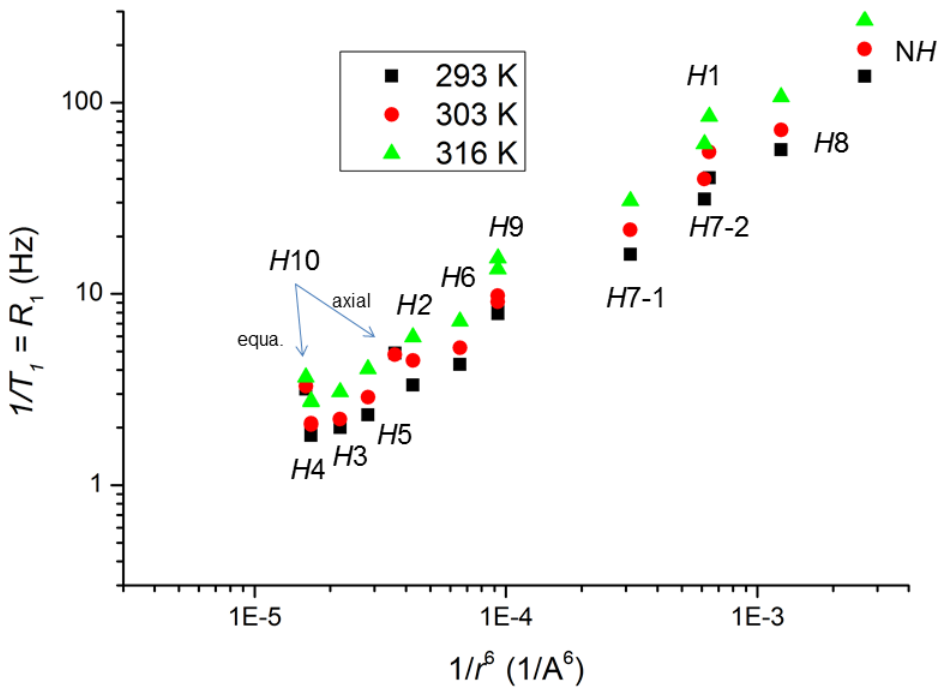

Figure 21-SI: Plot of the distance ($1/r^6$) of a particular proton from the metal center vs. the observed longitudinal relaxation rate R_1 for [Fe(*rac-trans*-**5**)]$^{2+}$. The logarithmic scale was used for sake of visual clarity.

The relaxation times resulting from Curie relaxation were calculated according to equation (12) for longitudinal relaxation time $T_1 = 1/R_1$ and equation (13) for the transversal relaxation times $T_2 = 1/R_2$.[2] The relaxation times resulting from dipolar relaxation were calculated according to equation (14) and (15).[2] The rotational correlation time τ_r was calculated to $\tau_r = 1.28 \cdot 10^{-10} s$ by the Einstein equation (11).[2] The electron relaxation time constant, τ_s, necessary for the calculation of the dipolar contribution to T_1, was determined by testing (equation (14)). Best results were obtained for $\tau_s = 1.2 \cdot 10^{-12} s$, well within the range expected for octahedral Fe^{2+} complexes.[2] All calculated relaxation times given in Table 10-SI were weighted by the appropriate HS fraction $\gamma_{HS}(T)$ (calculated from NMR data as $\gamma_{HS}(T)$ = 7.4 % at the temperature of the NMR probe (301 K corrected, 298 K (25°C) nominal). Relaxation due to contact coupling and relaxation within the LS species was neglected. Transversal relaxation times T_2 were calculated from the line widths at half height. They include the inhomogeneous broadening (usually < 1 Hz) as well as coupling to adjacent protons and are therefore termed T^*_2. For fast relaxing nuclei, the difference between

T_2 and T^*_2 can be associated to the possible scalar coupling to adjacent protons. The viscosity of acn was taken from tabulated data as η = 0.343 mPa s.[18]

For the calculations of the Curie relaxations, following formulae were used.

$$\tau_r = \frac{4\pi\,\eta\,a^3}{3\,k\,T};\ \eta = 0.343\ mPa\ s\ (viscosity\ acn);\ a = 7\ \text{Å}\ (a = radius\ of\ the\ complex\ )$$

$$\frac{1}{T_1} = \frac{2}{5}\left(\frac{\mu_0}{4\pi}\right)^2 \left\{\frac{\omega_I {g_e}^2 {\mu_B}^2 S(S+1)}{3kT}\right\}^2 \left\{\frac{1}{r^6}\right\}\left\{\frac{3\tau_r}{1+(\omega_I\tau_r)^2}\right\} \tag{12}$$

$$\frac{1}{T_2} = \frac{1}{5}\left(\frac{\mu_0}{4\pi}\right)^2 \left\{\frac{\omega_I {g_e}^2 {\mu_B}^2 S(S+1)}{3kT}\right\}^2 \left\{\frac{1}{r^6}\right\}\left\{4\tau_r + \frac{3\tau_r}{1+(\omega_I\tau_r)^2}\right\} \tag{13}$$

For dipolar relaxation the following equations were used:

$$\frac{1}{T_1} = \frac{2}{15}\left(\frac{\mu_0}{4\pi}\right)^2 \{{\gamma_I}^2 {g_e}^2 {\mu_B}^2 S(S+1)\}\left\{\frac{1}{r^6}\right\}\left\{\frac{6\tau_s}{1+\left((\omega_I+\omega_S)\tau_s\right)^2} + \frac{\tau_s}{1+\left((\omega_I-\omega_S)\tau_s\right)^2} + \frac{3\tau_s}{1+(\omega_I\tau_s)^2}\right\} \tag{14}$$

$$\frac{1}{T_2} = \frac{1}{15}\left(\frac{\mu_0}{4\pi}\right)^2 \{{\gamma_I}^2 {g_e}^2 {\mu_B}^2 S(S+1)\}\left\{\frac{1}{r^6}\right\}\left\{4\tau_s + \frac{6\tau_s}{1+\left((\omega_I+\omega_S)\tau_s\right)^2} + \frac{\tau_s}{1+\left((\omega_I-\omega_S)\tau_s\right)^2} + \frac{3\tau_s}{1+(\omega_I\tau_s)^2}\right\} \tag{15}$$

Herein, ω_I and ω_S are the proton and electron Larmor frequency, respectively, γ_I and γ_S are the gyromagnetic ratios for proton and electron, respectively.

Table 10-SI: Results of relaxation measurements of complex [Fe(*rac-trans*-**5**)]$^{2+}$ in d_3-acn solution.

Proton	T_1 (ms) (290 K)	T_1 (ms) (300.3 K)	T_1 (ms) (313 K)	Zn-H(Å)	$\frac{1}{r^6}\left(\frac{1}{Å^6}\right)$	T_1 calcd (300.3 K)		T_2 calcd (300.3 K)		T^*_2 obs. $^+$
						Curie (ms)	dip. (ms)	Curie (ms)	dip. (ms)	(ms)
*H*1	24.7	18.1	11.8	3.404	$642.8\cdot10^{-6}$	230	23	45	21.2	1.49
*H*7-1	61.9	46.2	32.6	3.839	$312.4\cdot10^{-6}$	480	48	94	43	1.93
*H*6	234	191	139	4.98	$65.6\cdot10^{-6}$	2300	229	446	207	7.96
*H*2	299	223	168	5.35	$42.6\cdot10^{-6}$	3500	352	685	319	13.3
*H*3	499	451	325	5.98	$21.9\cdot10^{-6}$	6800	687	1330	623	
*H*4	550	475	366	6.25	$16.8\cdot10^{-6}$	8800	895	1740	812	
*H*4	543	482	362	6.25	$16.8\cdot10^{-6}$	8800	895	1740	812	
*H*7-2	31.9	25.08	16.4	3.429	$615\cdot10^{-6}$	240	24	48	22	7.4
*H*5	429	346	247	5.73	$28.3\cdot10^{-6}$	5300	531	1035	482	32
*H*8	17.6	13.9	9.32	3.05	$1242\cdot10^{-6}$	120	12	24	10.9	7.4
NH	7.29	5.25	3.72	2.685	$2668\cdot10^{-6}$	60	5.6	11	5.1	4.2
*H*9-1	127	102	74	4.7	$93\cdot10^{-6}$	1600	161	320	147	
*H*10-1(eq.)	315	303	272	6.3	$16.0\cdot10^{-6}$	9300	938	1830	852	
*H*9-2	118	110	65	4.7	$93\cdot10^{-6}$	1600	161	320	147	
*H*10-2(ax.)	204	208		5.5	$36.1\cdot10^{-6}$	4100	415	810	377	

$^+$ calculated from the line widths; not corrected for eventual H,H-coupling.

1.6.1 Determination of the Exchange Time for the HS/LS Equilibrium

For the determination of the relaxation rate from the HS to LS state, the linewidths of the resonance signals were used. The linewidth was measured by fitting the resonances to a Lorentzian curve or by simulation with Dynamic NMR from the Topspin 2.1 program package. If possible, *H*,*H*-coupling was included (by Dynamic NMR). In addition, due to the fact that the transversal relaxation times $T^*{}_{2(obs)}$ are obtained by fitting a Lorentzian curve over the entire signal, they must be corrected for possible coupling with adjacent protons to yield $T_{2(obs)}$. Although not exactly correct, $T_{2(obs)}$ are the transversal relaxation times corrected for *H*,*H*-couplings. They were calculated by subtracting a reasonable value for the *H*,*H*-couplings, according to equation (16). It was assumed that the observed transversal relaxation rate $T_{2(obs)}$ is the sum of the weighted "natural relaxation rate" of a particular proton and the relaxation due to exchange broadening cause by the HS/LS equilibrium. Summation was done according to equation

(17). The expression used for the exchange broadening is an approximation valid for the fast exchange above the coalescence point.[19] The difference in the Larmor frequency of the proton in the pure HS and LS ($\Delta\omega$) states can be calculated from the fit parameters $C^1$and C^0 obtained from the calculations of ΔH and ΔS (18). Parameters C^1, C^0 and $\delta_{dia/LS}$ were refined as described in section 1.4.4.1 .

$$\frac{1}{T_{2(obs)}} = \frac{1}{T^*{}_{2(Lorentzian-fit)}} - \pi\ {}^{2,3}J(H,H) \tag{16}$$

$$\frac{1}{T_{2(obs)}} = \left\{(1-\gamma_{HS})\frac{1}{T_{2(LS)}} + \gamma_{HS}\frac{1}{T_{2(HS)}}\right\} + \left\{\gamma_{HS}(1-\gamma_{HS})\frac{\Delta\omega^2}{k_{ex}}\right\} \tag{17}$$

"natural line width (dipolar coupling)" exchange broadening

$$\Delta\omega = \omega_I\ (\ C^0/T + C^1) \tag{18}$$

The relaxation $T_{2(LS)}$ of proton spins in the pure LS-state was neglected. In order to calculate the transversal relaxation times $T_{2(HS)}$ of the pure HS-state, the ratio between the longitudinal relaxation times $T_{1(HS)}$ and the transversal relaxation times $T_{2(HS)}$ was estimated as 1.45 (from the calculation made above (Table 10)). Note that, with the assumptions made, this ratio only depends on the electron relaxation rate τ_s and the calculated rotational correlation time τ_r. With this ratio in hand, the linewidth expected for a particular proton without exchange broadening is calculated from the experimentally observed longitudinal relaxation time $T_{1(obs)}$ (equation (19)).

$$\gamma_{HS}\frac{1}{T_{2(HS)}} = \frac{1}{T_{1(obs)}}\frac{T_{2(HS)}}{T_{1(HS)}} \tag{19}$$

With this approach it is not necessary to assign the protons exactly and to identify the exact location of the proton relative to paramagnetic metal center; only the Curie constant C^0, C^1 (if refined) for a particular proton site to calculate $\Delta\omega$ (18) and $\Delta_{SCO}H$ as well as $\Delta_{SCO}S$, to calculate the exact HS-fraction $\gamma_{HS}(T)$, need to be known. The exchange rate k_{ex} for the SCO equilibrium can be calculated easily using equation (20).

$$k_{ex} = \left\{ \gamma_{HS}(1-\gamma_{HS}) \frac{\Delta\omega^2}{\frac{1}{T_{2(obs)}} - \frac{1}{T_{1(obs)}} \frac{T_{2(HS)}}{T_{1(HS)}}} \right\} \tag{20}$$

Table 11-SI: Results for relaxation time measurement (500 MHz) and calculations for complex [Fe(*rac-trans*-**5**)]$^{2+}$ in acn solution at 300.3 K.

Proton (300.3 K)	δ_{dia}	C^1 (ppm K)	C^0 (ppm)	C(300.2 K) (ppm K)	LW (Hz) #	$J^{H,H}$ (Hz) *	$J^{H,H}$ n.c. (Hz) +	T_1(ms)
*H*1	7.006	-24.3	55795	48553	214	5		18.1
*H*7-1	4.55	-8.36	44910	42418	165	12		46.2
*H*6	8.439	-2.603	20199	19423	40	7		191
*H*2	7.3929	0.846	13054	13306	24	7		223
*H*3	8.5054	-10.0357	7346	4355	(2.3)		12	451
*H*4	8.317	1.6477	4622	5113	(3)		9	475
*H*4	8.5794	6.17	1027	2865	(1.5)		9	482
*H*7-2	3.7755	-13.19	17285	13354	32	12		25.1
*H*5	9.023	5.489	-10078	-8442	10	0		346
*H*8	1.9657	-9.08288	13606	10899	43	12		13.9
NH	2.9149	1.295	4319	4704	73	0		5.25
*H*9-1	2.3136	-12.12	9730	6118	(4.5)			101.9
*H*10-1(eq.)	1.639	-5.49	7958	6321	(4)			303.7
*H*9-2	0.8469	-7.337	6576	4389	(2.5)			109.9
*H*10-2(ax.)	1.05873	-8.5211	5094	2554	(1.1)			208

linewidths which are too small to be used in the calculation are given in red in parentheses
* coupling constants that have been included in the calculation
+ coupling constants only given for reference

Table 12-SI: Continuation of results of relaxation time measurement and calculations for complex [Fe(*rac-trans*-**5**)]$^{2+}$ in acn solution at 300.3 K.

Proton (300.3 K)	R_2+R_{ex} (Hz)	R_1 (Hz)	$R_{2(dip+curie)}^{calcd.}$(Hz)	R_{ex} (Hz)	$\Delta\omega^2$ (Hz^2)	$\Delta\omega^2/R_{ex}$ (Hz)	k_{ex} (s^{-1})	τ_{ex}(ns)*
*H*1	657	55.2	80.0	576.6	$2.57\ 10^{+11}$	$4.32\ 10^{+8}$	$3.07\ 10^{7}$	32.6
*H*7-1	481	21.7	31.4	449.2	$1.97\ 10^{+11}$	$4.46\ 10^{+8}$	$3.01\ 10^{7}$	33.2
*H*6	104	5.2	7.6	96.1	$4.13\ 10^{+10}$	$4.43\ 10^{+8}$	$2.95\ 10^{7}$	33.8
*H*2	53	4.5	6.5	46.9	$1.94\ 10^{+10}$	$4.43\ 10^{+8}$	$2.84\ 10^{7}$	35.2
*H*3		2.2	3.2					
*H*4		2.1	3.1					
*H*4		2.1	3.0					
*H*7-2	63	39.9	57.8	5.0	$1.94\ 10^{+10}$	$4.11\ 10^{+8}$	$2.63\ 10^{+8}$	3.8
*H*5	32	2.9	4.2	27.5	$7.78\ 10^{+9}$	$2.75\ 10^{+8}$	$2.06\ 10^{+7}$	48.5
*H*8	97	72.0	104.4	<0	$1.30\ 10^{+10}$	-	-	-
NH	239	190.5	276.2	<0	$2.43\ 10^{+9}$	-	-	-
*H*9-1		9.8	14.2					
*H*10-1(eq.)		3.3	4.8					
*H*9-2		9.1	13.2					
*H*10-2(ax.)		55.2	80.0					

* average for *H*1, *H*7-1, *H*6 and *H*2 is calculated as τ_{ex} = 33.7 ns

Table 13-SI: Summary of the relaxation time measurements in acn solution and calculations of chemical exchange at 293 K for complex [Fe(*rac-trans*-**5**)]$^{2+}$.

Proton (293 K)	LW (Hz) @500 MHz	LW (Hz) @250 MHz	LW (Hz) @250 MHz calcd.	T_1 (ms)	R_2+R_{ex} (Hz)	R_1 (Hz)	$R_{2(dip+curie)}^{calcd.}$ (Hz)	R_{ex} (Hz)	k_{ex} (s^{-1})	τ_{ex}(ns)
*H*1	212	65	71	24.7	666	40.5	58.7	591.6	2.42 10^7	41.3
*H*7-1	170	55	57	61.95	534	16.1	23.4	473.0	2.31 10^7	43.3
*H*6	40	18	17	234	126	4.3	6.2	97.5	2.35 10^7	42.6
*H*2	25	16	13	299	79	3.3	4.8	51.7	2.07 10^7	48.3
*H*7-2	41	32	30	31.9	129	31.4	45.5	45.6	1.74 10^7	57.6
*H*5	10			429	31	2.3	3.4	28.0	1.60 10^7	62.5
*H*8	40	36	39	17.6	126	56.7	82.2	5.7	2.26 10^7	44.3
NH	56	54	-	7.3	176	137.2	198.9	<0	-	-

Table 14-SI: Summary of the relaxation time measurements in acn solution and calculations of chemical exchange at 316 K for complex [Fe(*rac-trans*-**5**)]$^{2+}$.

Proton (316.07 K)	LW (Hz) @500 MHz	T_1 (ms)	R_2+R_{ex} (Hz)	R_1 (Hz)	$R_{2(dip+curie)}^{calcd.}$ (Hz)	R_{ex} (Hz)	k_{ex} (s^{-1})	τ_{ex}(ns)
*H*1	260	11.8	810.5	84.8	122.9	678,2	3.80 10^7	26.3
*H*7-1	192	32.6	549.8	30.7	44.5	555,6	3.59 10^7	27.9
*H*6	51	139	133.5	7.2	10.4	127,8	3.27 10^7	30.6
*H*2	31	168	70.7	5.9	8.6	66,8	2.96 10^7	33.8
*H*7-2	50	16.4	147.7	61.0	88.4	31,0	6.40 10^7	15.6
*H*5	12	247	37.7	4.05	5.9	31,8	2.57 10^7	38.8
*H*8	60	9.32	150.8	107.3	155.6	<1	-	-
NH	100	3.72	314.2	268.8	389.8	<1	-	-

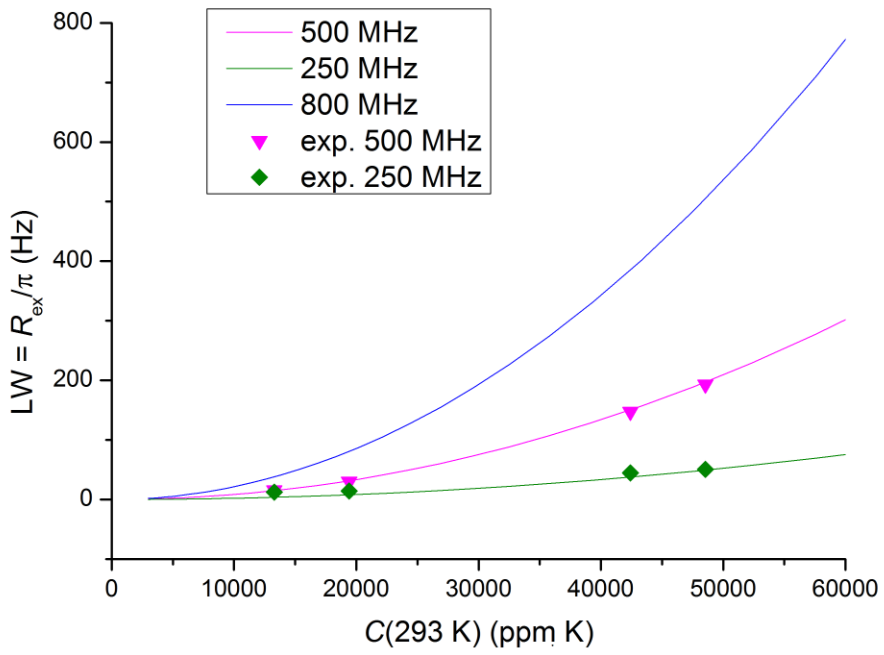

Figure 22-SI: Calculated broadening of the resonance due to the chemical exchange between HS and LS state for different Curie constants. Exchange rate constant (τ_{ex} = 43ns) and HS-fraction (5.3% HS) obtained for complex [Fe(*rac-trans*-**5**)]$^{2+}$ at 293 K. Points represent experimentally obtained broadening for *H*2, *H*6, *H*7-1 and *H1* respectively (from left to right).

1.7 Possible Simplification and Advantages of the NMR Method

A major advantage of using chemical shifts to evaluate thermodynamic SCO parameters is the high resolution. Chemical shifts can be measured with a resolution of less than 0.1 ppm within a possible range more than 100 ppm; that is, resolution is better than 1‰. This should be compared with the resolution that can be obtained *via* UV/Vis spectroscopy, where typical molar absorption coefficients of ca. 10^4 M^{-1} s^{-1} are known with a far less precision; that is, resolution is below 1%. Furthermore, the NMR-spectroscopic approach relies on very convenient sample preparation routines, as chemical shifts do not depend on the concentration so that solvent-density corrections are not necessary. Moreover, chemical shifts are specific for a component, so that impurities have little effect on the results,[20] and even mixtures of spin crossover complexes can be investigated. Also for very rough estimations the VT ^{1}H-NMR spectroscopy can be profitable. A closer look at Figure 2 in the main paper showed that the curve of $\delta_{obs}(T)$ over T has a positive slope, for a positive Curie constant, up to a HS-fraction of 80%. An inflexion point is found at a HS fraction of about 40 %. This allows a rough but straightforward estimation of the HS fraction.

In this survey the extraction of the kinetics from the NMR spectra is described in detail and therefore it seems complex, but it can be very straight-forward with some simplifications. Before any calculations are started, it should be clarified that the complex is stable enough in solution to obtain reliable data. This is done by the addition of free ligand (10 mol%). A substantial ligand exchange on the NMR time scale will lead to broadening of the resonances for the free ligand. d_5-Nitrobenzene and d_6-acetone are good choices as solvents. Both are commercially available and do not form stable complexes with Fe^{2+}. The first problem of the calculation is determination of the HS fraction. Here we used the NMR spectroscopy to deduce γ_{HS} but also other means are suitable like UV/Vis spectroscopy or the classical Evans method. $\delta_{dia/LS}$ can be estimated from a zinc analog e. g. [Zn(*rac*-*trans*-**5**)]$^{2+}$ or simply from the free ligand. With this in hand and with the Curie constant y_{HS} can be calculated from the observed chemical shift using the averaged C^0, (C^1 = 0) from Table 3-SI. Subsequently we can calculate the chemical shift of the SCO complex in the HS state and similarly also $\Delta\omega$ ($\Delta\omega = (\delta_{obs} - \delta_{dia/LS})/(1-\gamma_{HS})$). The next problem is the calculation of the natural linewidths. We ignore relaxation in LS state and calculate the natural linewidths $R_2 = R_1 \cdot T_2/T_1$, R_1 is taken from T_1 measurements.

The ratio T_2/T_1 was calculated as 1.45 this is a rather typical value, likely for all octahedral Fe^{2+} complexes with nitrogen donors. This is a good estimate for most of the mononuclear Fe^{2+}-SCO complexes. In many cases suitable HS complexes can serve as model and directly provide the $R_{2(HS)}$ without any relaxation measurements. This transfer is justified within a series of complexes with similar size and coordination sphere. With the known linewidths, δ_{obs}, $\delta_{dia/LS}$, γ_{HS} and $R_{2(HS)}$ the kinetics k_{ex} and subsequent k_{LH} and k_{HL} can be calculated using equation (17). This is outlined in Table 15-SI for most suitable protons *H*1 and *H*7-1. The agreement with laser flash photolysis experiment is still acceptable. Many different schemes to extract kinetics from NMR spectra can be envisioned depending on the available data and model complexes.

Table 15-SI: summary of rough calculations of exchange rate k_{ex} for complex [Fe(*rac-trans*-**5**)]$^{2+}$.

	$\delta_{dia/LS}$ (Zn^{2+})[a] (ppm)	δ_{obs} [a] (ppm)	LW [a] (Hz)	T_1 [b] (ms)	C^0 [c] (ppmK)	$\Delta\omega$ [d] (Hz)	y_{HS} γ_{LS} [e]	y_{HS} $R_{2(HS)}$ (Hz)	k_{ex}(Mhz)/τ_{ex} (ns)
*H*1	8.09	19.17	210	24.7	46821	4.9 10^5	0.066	58.7	26.4/38
*H*7-1	4.53	15.19	150	62.0	42176	4.4 10^5	0.070	23.4	30.5/33

a) see section 1.1 b) see Figure 4 in the main paper c) see section 1.4.5 d) 2 π C^0/T (T = 300K) e) $\gamma_{HS} = (C^0/T)/(\delta_{obs}-\delta_{dia})$ f) = $(1/T_1)$ 1.45 see 1.6

It is worth to note that laser flash photolysis relies on a suitable absorption band that allows the excitation to the HS state and match the wavelength of the available laser; the NMR method is not subject to such restrictions.

1.8 NMR Spectra of [Fe(cis-5)]$^{2+}$

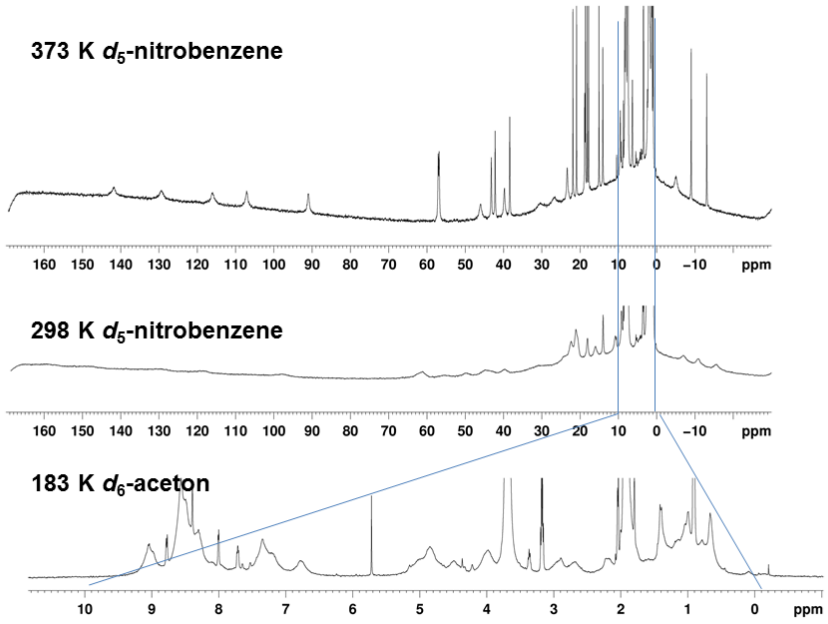

Figure 23-SI: NMR spectra of complex [Fe(*cis*-**5**)]$^{2+}$. Spectrum at the top was recorded in d_5-nitrobenzene at 373 K. The number of resonances agrees with the expected C_1 symmetric structure. The spectrum in the middle was also recorded in d_5-nitrobenzene but at 298 K. In contrast to the other investigated Fe^{2+}-SCO-complexes the resonances in this spectrum of [Fe(*cis*-**5**)]$^{2+}$ are unusually broadened. The spectrum at the bottom was measured in d_6-acetone at 183 K. The resonances found for [Fe(*cis*-**5**)]$^{2+}$ all fall in the diamagnetic region. Moreover all resonances show similar line broadening effect. This abnormality points to a slow decay of the initially present LS-species to a HS-species with the time constant $\tau \approx 5$ ms of (LW ≈°70Hz).

1.9 Laser-Excitation and Relaxation Measurements

Nanosecond LFP experiments were performed with the laser wavelength 532 nm of a Nd:YAG laser system, as described in detail elsewhere.[21] Decay profiles of transient absorption of [Fe(*rac-trans*-**5**)]$^{2+}$ and [Fe(*rac-trans-NMe*-**5**)]$^{2+}$ were recorded in MeOH and acn at λ_{obs} = 570 nm, corresponding to the maximum of the ground-state MLCT absorption of the complex ions. The pulse duration of 8 ns with an energy of *ca.* 10 mJ per pulse was much shorter than the decay lifetimes of the transient signals, so that deconvolution was not required for kinetic analysis. Before each measurement, the solutions in high-purity methanol and acetonitrile ($OD_{532} \approx 0.5$; concentrations in the range 1

× 10^{-4} M) were rigorously deoxygenated by flushing with analytical grade argon for 20 minutes prior to measurement, under argon, in sealed quartz cuvettes.

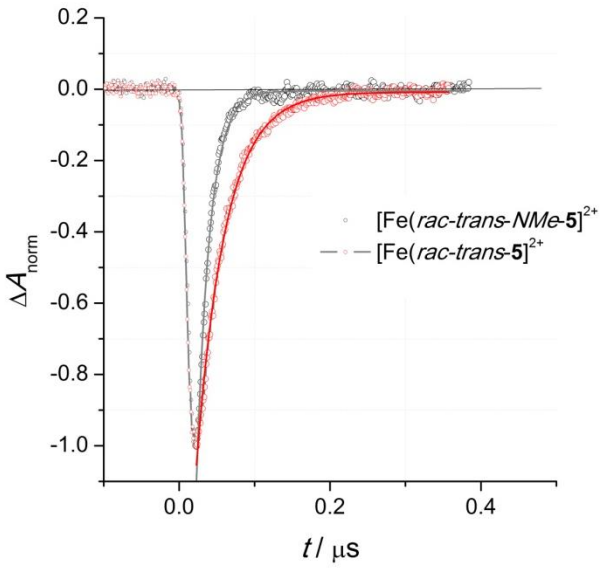

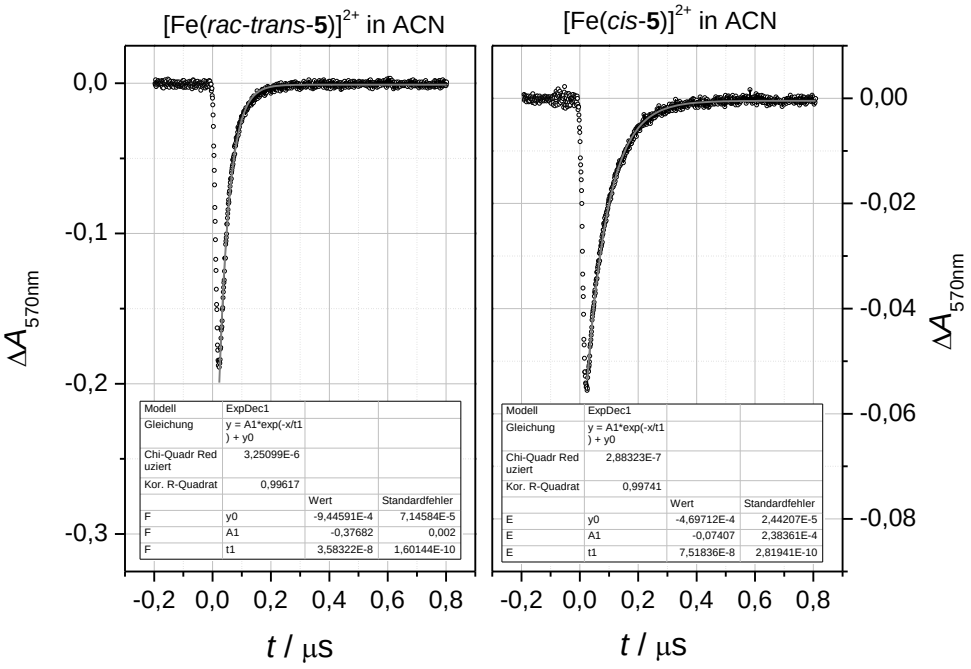

Figure 24-SI: Recovery profiles of transient absorption recorded at λ_{obs} = 570 nm after flashing (λ_{exc} = 532 nm) complex solutions @ ambient temperature; **Top:** Profiles of [Fe(*rac-trans*-**5**)]$^{2+}$ (red) and [Fe(*rac-trans-NMe*-**5**)]$^{2+}$ (black) in MeOH; **Bottom:** Profiles of [Fe(*rac-trans*-**5**)]$^{2+}$ (left) and [Fe(*cis*-**5**)]$^{2+}$ (right) in acn; symbols: experimental data; lines: mono-exponential fits; results of fitting are given in the boxes.

1.10 X-ray Structure Determination

Crystals suitable for single crystal analyses were grown by slow diffusion of diethyl ether into a solution of the appropriate complex in acn. Reflection data have been collected on an Oxford Gemini S diffractometer with graphite-monochromatized Mo Kα radiation (λ = 0.71073 Å, [Fe(*cis*-**5**)]$(BF_4)_2$·(CH_3CN) and [Zn(*rac-trans*-**5**)]$(ClO_4)_2$·(CH_3CN)**,** [Zn(*R,R*-**5**)][Fe(*S,S*-**5**)]$(ClO_4^-)_4$·(CH_3CN)**,** [Fe(*rac-trans-NMe*-**6**)]$(BF_4)_2$) and Cu Kα radiation (λ = 1.54184 Å, [Fe(*rac-trans-NMe*-**5**)]$(BF_4)_2$·(0.5·CH_3CN)) at 110 K ([Fe(*rac-trans-NMe*-**5**)]$(BF_4)_2$·(0.5·CH_3CN) and [Zn(*R,R*-**5**)][Fe(*S,S*-**5**)]$(ClO_4^-)_8$·(CH_3CN)), 115 K ([Fe(*rac-trans-NMe*-**6**)]$(BF_4)_2$) and 150 K ([Fe(*cis*-**5**)]$(BF_4)_2$·(CH_3CN) and [Zn(*rac-trans*-**5**)]$(ClO_4)_2$·(CH_3CN)). All structures were solved by direct methods and refined against IF_oI^2 with SHELXS-2013 and SHELXL-2013,[22] respectively. All non hydrogen and non solvent atoms were refined anisotropically. Hydrogen atoms were placed at calculated positions with a riding model except for the secondary amine hydrogen atoms: bound to N1 in [Zn(*rac-trans*-**5**)]$(ClO_4)_2$·(CH_3CN), bound to N1 and N4 in [Zn(*R,R*-**5**)][Fe(*S,S*-**5**)]$(ClO_4)_4$·(CH_3CN) and [Fe(*cis*-**5**][$(BF_4)_2$·(CH_3CN). The positions of these hydrogen atoms were taken from difference Fourier maps and refined isotropically. In case of [Fe(*cis*-**5**)]$(BF_4)_2$·(CH_3CN) one BF_4^- anion (B1, F1-F4) was refined disordered with split occupancies of 0.36/0.64. In case of [Fe(*rac-trans-NMe*-**5**)]$(BF_4)_2$·(0.5·CH_3CN) two BF_4^- anions (B3, F9-F12 and B4, F13-F16) were refined disordered with split occupancies of 0.47/0.53 and 0.5/0.5, respectively. Furthermore, the asymmetric unit of [Fe(*rac-trans-NMe*-**5**)]$(BF_4)_2$·(0.5·CH_3CN) comprises two crystallographically different cations [Fe(*rac-trans-NMe*-**5**)]$^{2+}$. During data collection of [Fe(*rac-trans-NMe*-**5**)]$(BF_4)_2$·(0.5·CH_3CN), the measurement of standard frames did indicate a slight decay of intensity. This is attributed to the loss of packing solvents (diethyl ether and acetonitrile). Indeed, a reliable refinement was possible only by using the SQUEEZE procedure (cf. above), by which an electron count of 544 electrons/cell were omitted. These correspond approximately to three molecules diethyl ether and one molecule acn. Therefore, the crystal structure comprises comparatively large VOIDS.

In case of [Zn(*R,R*-**5**)][Fe(*S,S*-**5**)]$(ClO_4)_4$·(CH_3CN), an acn molecule (N1N, C1N, C2N) as packing solvent has been refined disordered with split occupancies of each 0.25, resulting in a partial occupation of 0.5. Furthermore, the space group *I*2 was chosen so that the two complex cations [Zn(*R,R*-**5**)]$^{2+}$ and [Fe(*S,S*-**5**)]$^{2+}$ were refined

independently. This excludes some suggested symmetry operations (centers of inversion). It is generally difficult to distinguish between Zn^{2+} and Fe^{2+} in standard single crystal x-ray structure analyses. Therefore we checked the original crystal after the collection of the data by ESI-MS and found the expected 1:1 mixture of [Zn(*R,R*-**5**)]$^{2+}$ and [Fe(*S,S*-**5**)]$^{2+}$. Eventually, the Fe-N and Zn-N bond length were refined without any constrains and yield the typical bond lengths for Zn^{2+} and LS-Fe^{2+} in the correct enantiomer. Therefore we exclude the possibly of a substantial ligand scrambling between [Zn(*R,R*-**5**)]$^{2+}$ and [Fe(*S,S*-**5**)]$^{2+}$ during the process of crystallization (2 months at ambient temperature). In order to test ligand scrambling between [Zn(rac-trans-**5**)]$^{2+}$ and [Fe(rac-trans-**5**)]$^{2+}$, an acn solution of colourless [Zn(rac-trans-**5**)]$^{2+}$ and an excess of $[Fe(H_2O)_6](ClO_4)_2$ was refluxed, the solution remained colourless. This shows that ligands scrambling is indeed extremely slow.

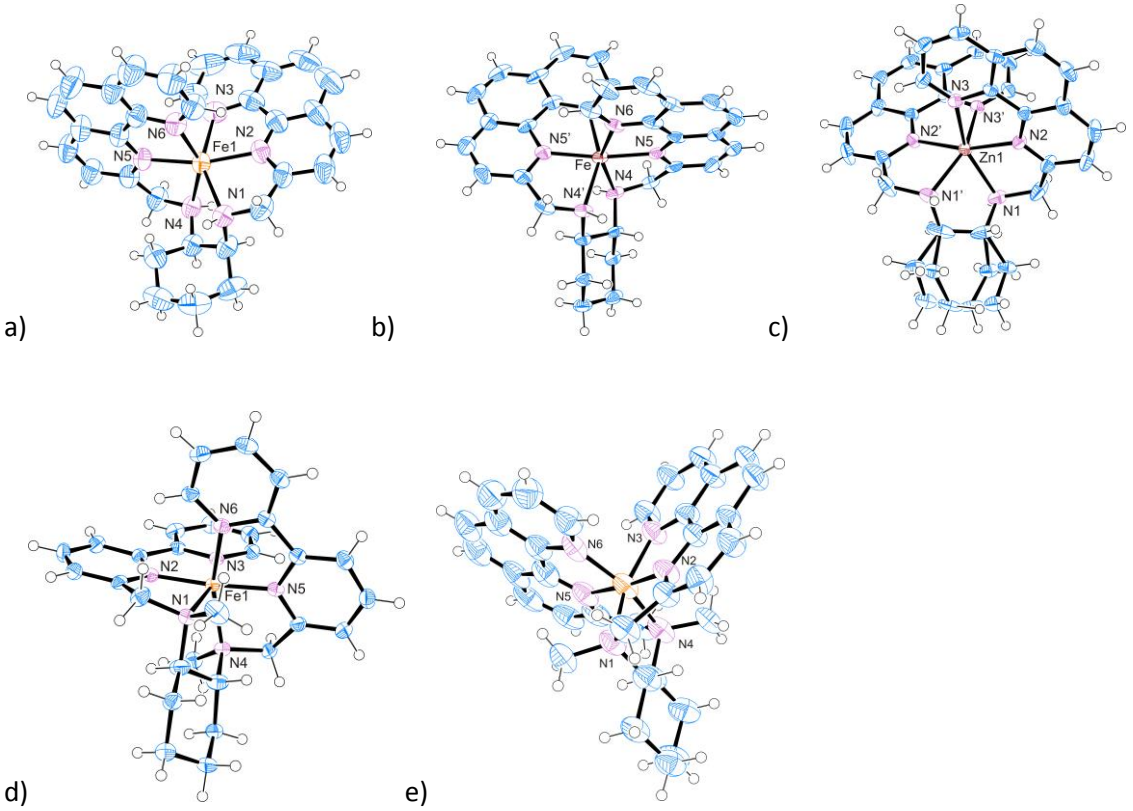

Figure 25-SI: Molecular structure of a) the complex cation [Fe(*cis*-**5**]$^{2+}$ in [Fe(*cis*-**5**][$(BF_4^-)_2$·(CH_3CN); b) the complex cation [Fe(S,S-**5**]$^{2+}$ in [Zn(*R,R*-**5**)][Fe(*S,S*-**5**)]$(ClO_4)_4$·(CH_3CN); c) the complex cation [Zn(*rac-trans*-**5**] in [Zn(*rac-trans*-**5**)]$(ClO_4)_2$·(CH_3CN); d) the complex cation [Fe(*rac-trans*-

NMe-**6**]$^{2+}$ and e) the complex cation [Fe(*rac-trans-NMe*-**5**]$^{2+}$ in [Fe(*rac-trans*-NMe-**5**)]$(BF_4)_2$·(0.5·CH_3CN). For details of the labeling scheme see Figure 27.

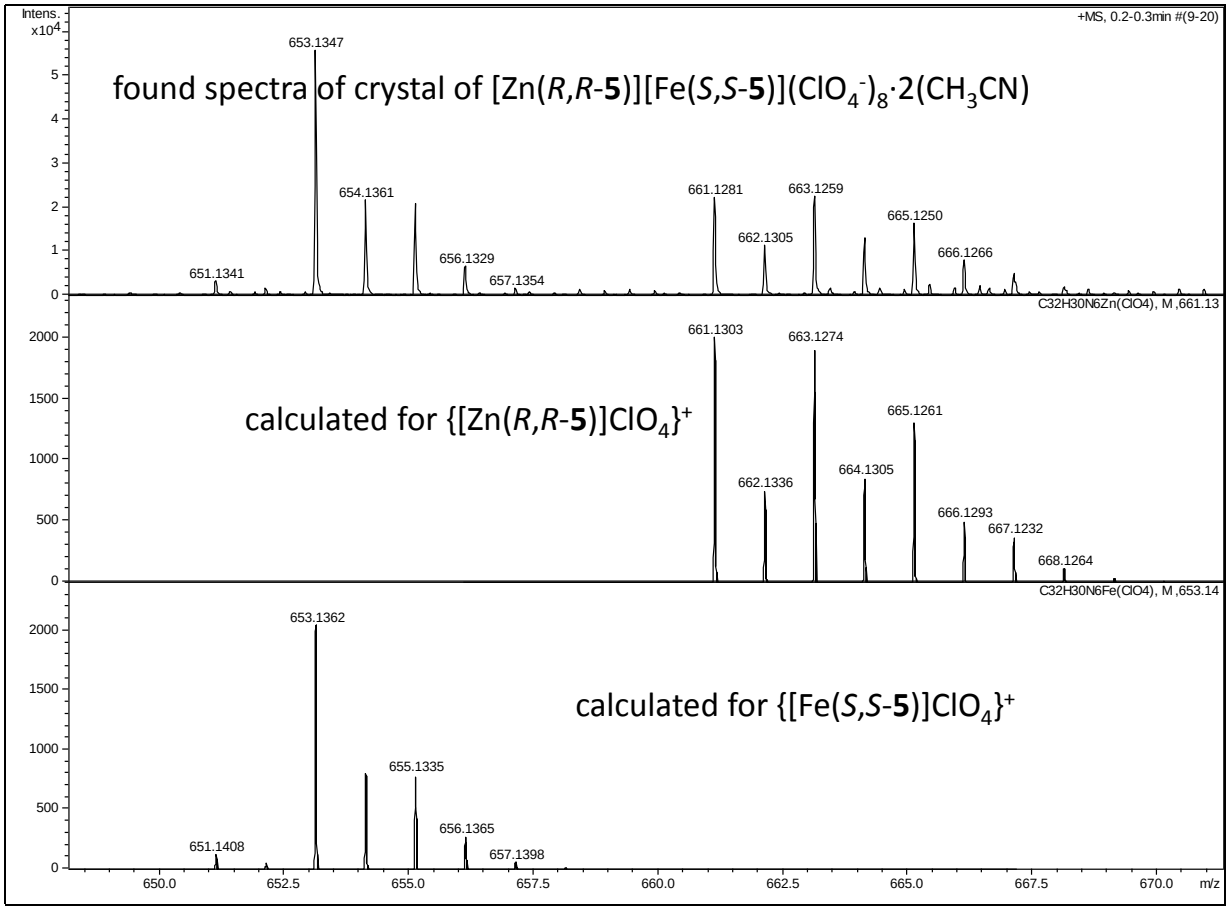

Figure 26-SI: ESI-MS obtained from original crystal of [Zn(*R,R*-**5**)][Fe(*S,S*-**5**)]$(ClO_4)_4$·(CH_3CN) (top) used for the x-ray structure determination and the calculted pattern for the most likely fragment peaks {[Zn(*R,R*-**5**)]ClO_4}$^+$ (middle) {[Fe(*S,S*-**5**)]ClO_4}$^+$ (bottom) of single components.

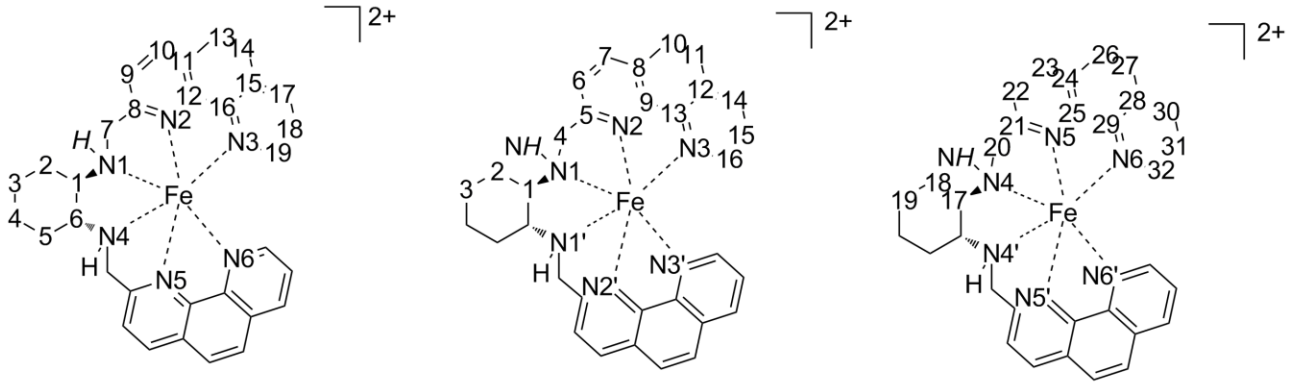

C_1-symmetric

[Fe(rac-*trans-NMe*-**5**)]$^{2+}$
[Fe(cis-**5**)]$^{2+}$
[Fe(rac-*trans-NMe*-**6**)]$^{2+}$

C_2-symmetric

[Zn(*S,S-trans*-**5**)]$^{2+}$
[Zn(*rac-trans*-**5**)]$^{2+}$

[Fe(*R,R-trans*-**5**)]$^{2+}$

Figure 27-SI: Labelling scheme used for presentation of the x-ray structures of crystallograpic C_1- and C_2-symmetric complexes.

Table 16-SI: data for crystal structure refinement.

	[Zn(*rac-trans*-**5**)] $(ClO_4)_2\cdot(CH_3CN)$	[Fe(*rac-trans*-NMe-**5**)]$(BF_4)_2$ $\cdot(0.5\cdot CH_3CN)$	[Fe(*cis*-**5**)]$(BF_4)_2$ $\cdot 0.5(CH_3CN)$	[Zn(*R*,*R*-**5**)] [Fe(*S*,*S*-**5**)]$(ClO_4)_4$ $\cdot(CH_3CN)$	[Fe(*rac-trans* -NMe-**6**)]$(BF_4)_2$
empirical formula	$C_{36}H_{36}Cl_2N_8O_8Zn$	$C_{70}H_{71}B_4F_{16}Fe_2N_{13}$	$C_{66}H_{63}B_4F_{16}Fe_2N_{13}$	$C_{128}H_{120}Cl_8Fe_2N_{24}O_{32}Zn_2$	$C_{30}H_{34}B_2F_8FeN_6$
formula weight (g/mol)	845.00	1553.34	1497.23	3114.62	708.10
T (K)	150	110	150	110	115
Wavelength (Å)	0.71073	1.54184	0.71073	0.71073	0.71073
crystal system. space group	monoclinic *C*2/c	monoclinic $P2_1/c$	monoclinic *C*2/c	monoclinic *I*2	monoclinic $P2_1/n$
unit cell dimensions					
a (Å)	23.4625(1)	14.2146(12)	36.181(3)	14.5861(3)	17.0747(5)
b (Å)	10.3557(2)	26.2737(19)	10.2086(6)	13.0946(3)	9.8281(3)
c (Å)	16.8781(4)	22.698(3)	19.477(2)	17.1156(3)	36.0100(11)
α (°)	90	90	90	90	90
β (°)	119.285(2)	101.469(10)	107.983(10)	99.518(2)	98.327(3)
γ (°)	90	90	90	90	90
volume	3576.78(13)	8307.7(13)	6842.4(10)	3224.06(12)	5979.2(3)
Z	4	4	8	1	8
absorption coefficient (cm^{-1})	0.902	3.501	0.519	0.846	0.589
F(000)	1744	3192	3064	1604	2912
Θ-range f. data coll. (°)	3.134 to 24.999	3.172 to 61.996	3.09 to 25.06	3.020 to 24.997	3.048 to 24.999
limiting indices	27 ≤ h ≤ 27 -12 ≤ k ≤ 12 -20 ≤ l ≤ 18	-16 ≤ h ≤ 16 -26 ≤ k ≤ 30 -26 ≤ l ≤ 26	-42 ≤ h ≤ 41 -10 ≤ k ≤ 12 -23 ≤ l ≤ 19	-17 ≤ h ≤ 17 -15 ≤ k ≤ 13 -20 ≤ l ≤ 19	-19 ≤ h ≤ 20 -11 ≤ k ≤ 11 -42 ≤ l ≤ 42
reflections coll. / unique	13625 / 3132 [R_{int} = 0.0247]	24177 / 12715 [R_{int} = 0.0693]	23852 / 6002 [R_{int} = 0.1108]	14257 / 5241 [R_{int} = 0.0205]	46925 / 10500 [R_{int} = 0.0373]
data / restraints / parameters	3132/9/273	12715/1131/1039	6002/54/523	5241/73/499	10519/0/847
GooF on F^2	1.093	0.923	1.053	1.019	1.022
final R indices ($I > 2\sigma(I)$)	*R*1 = 0.0365 w*R*2 = 0.1004	*R*1 = 0.0851 w*R*2 = 0.2101	*R*1 = 0.0701 w*R*2 = 0.1970	*R*1 = 0.0317 w*R*2 = 0.0809	*R*1 = 0.0522 w*R*2 = 0.1224
(all data)	*R*1 = 0.0428 w*R*2 = 0.1023	*R*1 = 0.1405 w*R*2 = 0.2481	*R*1 = 0.0842 w*R*2 = 0.2144	*R*1 = 0.0361 w*R*2 = 0.0840	*R*1 = 0.0634 w*R*2 = 0.1273
abs. structure para.[23,24]				0.021(7)	
larg. diff. peak and hole ($e^-/Å^3$)	0.803 and -0.469	0.758 and -0.498	0.510 and -0.496	0.387 and -0.315	0.693 and -0.506

Table 17-SI: selected bond lengths and angles

	[Zn(*rac-trans*-**5**)] $(ClO_4)_2 \cdot (CH_3CN)$	[Fe(*rac-trans*-NMe-**5**)]$(BF_4)_2$ $\cdot(0.5 \cdot CH_3CN)$	[Fe(*cis*-**5**][$(BF_4)_2$ $\cdot(CH_3CN)$	[Zn(*R*,*R*-**5**)][Fe(*S*,*S*-**5**)] $(ClO_4)_4$ $\cdot(CH_3CN)$	[Fe(**6**)]$(BF_4)_2$
Comments	C_2-symmetric	C_1-symmetric	C_1-symmetric	C_2-symmetric M_1 = Zn / M_2 = Fe	C_1-symmetric
bond lengths					
M_1-$N_{1/4}$	2.188(2)	2.084(5)	2.227(3)	2.178(5)	2.071(2)
M_1-$N_{2/5}$	2.0552(19)	1.871(5)	2.106(3)	2.038(4)	1.892(3)
M_1-$N_{3/6}$	2.2841(19)	2.005(5)	2.253(4)	2.227(5)	1.984(2)
M_2-N_4		2.067(6)	2.219(3)	2.067(4)	2.058(3)
M_2-N_5		1.890(5)	2.100(3)	1.899(4)	1.889(2)
M_2-N_6		1.987(6)	2.223(3)	2.010(4)	1.973(2)
angles					
N1-N4		2.8297(4)	2.865(4)		2.800(4)
N1-N1’	2.890			2.8779(1) (M_1)	
N4-N4’				2.7794(1) (M_2)	
torsion angles					
N1-M_1-N4/1’	82.65(13)	85.5(2)	80.3(1)	82.7(3)	85.4(1)
N2-M_1-N5/2’	164.53(11)	175.2(2)	165.5(1)	171.1(3)	175.1(1)
N3-M_1-N6/3’	93.58(9)	91.4(2)	91.4(1)	96.9(2)	94.9(1)
N4-M_2-N4’				84.5(2)	
N5-M_2-N5’				175.5(3)	
N6-M_2-N6’				97.6(2)	
N1-C1-C6-N4		53.15	60.6		51.3(4)
N1-C1-C1’-N1’	64.41			53.19	
N4-C17-C17-N4’				54.46	

1.11 Electrochemical Measurements

Acetonitrile (analytical grade) was available from Acros Organics and stored over molecular sieve (4 Å). $[N^nBu_4][B(C_6F_5)_4]$ was prepared by metathesis of $Li[B(C_6F_5)_4]\cdot nEt_2O$ (Boulder Scientific) with $[N^nBu_4]Br$ according to a published procedure.[25] Its purification was enhanced by a filtration step of the crude product through a pad of silica using dichloromethane as a solvent.

For electrochemical measurements, a Voltalab 10 electrochemical laboratory from Radiometer Analytical was used. All experiments were carried out under an atmosphere of argon on acetonitrile solutions of the analyte (≈1 mM), containing 0.1 mol·L^{-1} of $[N^nBu_4][B(C_6F_5)_4]$ as supporting electrolyte.[26,27] For voltammetry, a three electrode cell with a platinum auxiliary electrode, a glassy carbon working electrode (3.0 mm in diameter) and a Ag/Ag^+ reference electrode were used. The working electrode was prepared by polishing with Buehler MicroFloc using Buehler diamond suspensions with decreasing sizes (1 to 0.25 µm). The Ag/Ag^+ reference electrode was constructed from a silver wire inserted into a Luggin capillary with a Vycor tip containing a solution of 0.01 mol·L^{-1} $[AgNO_3]$ and 0.1 mol·L^{-1} of the supporting electrolyte in acetonitrile. This Luggin capillary was inserted into a second Luggin capillary with a Vycor tip filled with a 0.1 mol·L^{-1} supporting electrolyte solution in acetonitrile. Successive experiments under the same experimental conditions showed that all formal reduction and oxidation potentials were reproducible within ±5 mV. Experimentally potentials were referenced against a Ag/Ag^+ reference electrode, but the results are presented referenced against the FcH/FcH^+ couple ($E^{0\prime}$ = 0.0 V) as required by IUPAC.[28] Within this context, decamethylferrocene was used as an internal standard and the experimentally measured potentials were converted into *E vs* FcH/FcH^+ by addition of –0.51 V.[29,30] The cyclic voltammograms were taken typically after two scans and are considered to be steady state cyclic voltammograms, in which the signal pattern differs not from the initial sweep. Finally, the experimental data were processed on Microsoft Excel worksheets.

Table 18-SI: Results of electrochemical measurement obtained for the redox pair $[Fe(\mathbf{5}/\mathbf{6})]^{2+}$. Potentials are referenced to the ferrocene/ferrocenium redox couple.

	$E^{0\prime}$	ΔE_p
$[Fe(rac\text{-}trans\text{-}\mathbf{5})](PF_6)_2$	465 mV	65 mV

[Fe(*rac-trans-NMe*-**5**)]$(BF_4)_2$	570 mV	65 mV
[Fe(*cis*-**5**)]$(ClO_4)_2$	487 mV	109 mV
[Fe(*rac-trans-NMe*-**6**)]$(BF_4)_2$	540 mV	65 mV

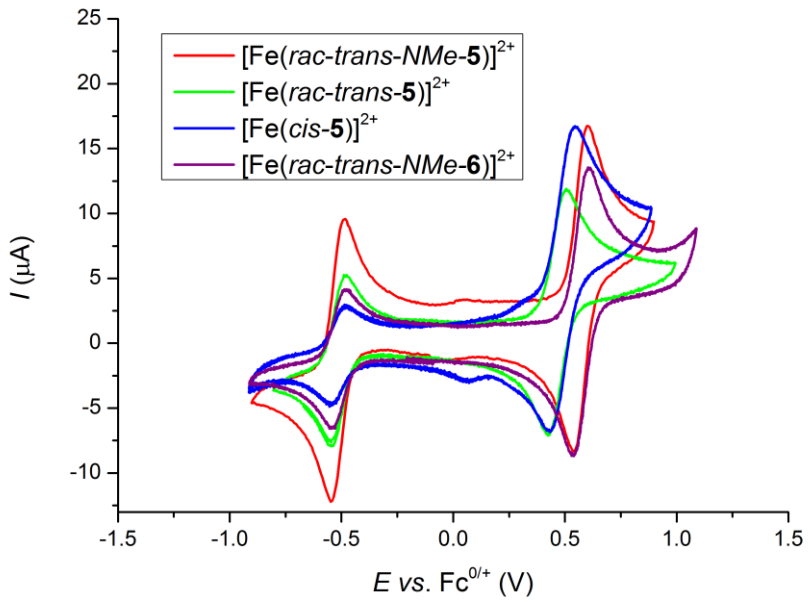

Figure 28 -SI: Cyclic voltammograms obtained for the redox pair [Fe(**5**/**6**)]$^{2+}$. Potentials are referenced to the ferrocene/ferrocenium redox couple. Shown with internal standard decamethylferrocene (-0.51 V).

[1] E. C. Constable, G. Zhang, C. E. Housecroft, M. Neuburger, J. A. Zampese, *Eur. J. Inorg. Chem.* **2010**, 2000–2011.

[2] G. P. I. Bertini C. Luchinat, *Solution NMR of Paramagnetic Molecules*, Elsevier, **2001**.

[3] A. L. Van Geet, *Anal. Chem.* **1970**, *42*, 3–4.

[4] H. F. G. Schilling, *Org. Magn. Reson.* **1979**, *12*, 569–573.

[5] K. Bryliakov, E. Duban, E. Talsi, *Eur. J. Inorg. Chem.* **2005**, 72–76.

[6] P. Basu, N. V Shokhirev, J. H. Enemark, F. A. Walker, **1995**, 9042–9055.

[7] Z. Xia, B. D. Nguyen, G. N. La Mar, *J. Biomol. NMR* **2000**, *17*, 167–74.

[8] B. Weber, C. Carbonera, C. Desplances, J.-F. Letard, *Eur. J. Inorg. Chem.* **2008**, 1589–1598.

[9] B. Weber, F. A. Walker, *Inorg. Chem.* **2007**, *46*, 6794–803.

[10] B. Weber, J. Obel, D. Henner-Vasquez, W. Bauer, *Eur. J. Inorg. Chem.* **2009**, 5527–5534.

[11] B. Weber, E. S. Kaps, J. Obel, K. Achterhold, F. G. Parak, *Inorg. Chem.* **2008**, *47*, 10779–10787.

[12] H. E. Gottlieb, V. Kotlyar, A. Nudelman, **1997**, *3263*, 7512–7515.

[13] E. C. Constable, G. Baum, E. Bill, R. Dyson, R. v. Eldik, D. Fenske, S. Kaderli, D. Morris, A. Neubrand, M. Neuburger, et al., *Chem. Eur. J.* **1999**, *5*, 498–508.

[14] M. Chergui, in *Spin-Crossover Mater.* (Ed.: M.A. Halcrow), John Wiley & Sons, **2013**, pp. 405–420.

[15] S. Heider, H. Petzold, J. M. Speck, T. Rüffer, D. Schaarschmidt, *Zeitschrift für Anorg. und Allg. Chemie* **2014**, *640*, 1360–1367.

[16] H. Petzold, S. Heider, *Eur. J. Inorg. Chem.* **2011**, *2011*, 1249–1254.

[17] *CRC Handbook*, Taylor & Francis Group, **2015**.

[18] "Acetonitrile (data page)," can be found under https://en.wikipedia.org/wiki/Acetonitrile_(data_page), **2016**.

[19] J. S. Leigh, *J. Magn. Reson.* **1971**, *311*, 308–311.

[20] E. Sinn, *Inorganica Chim. Acta* **1969**, *3*, 11–16.

[21] T. Pedzinski, A. Markiewicz, B. Marciniak, *Res. Chem. Intermed.* **2009**, *35*, 497–506.

[22] G. M. Sheldrick, *Acta Cryst.* **2008**, *A64*, 112–122.

[23] H. D. Flack, G. Bernardinelli, **2000**, 1143–1148.

[24] H. D. Flack, *Acta Crystallogr., Sect. A Found. Crystallogr.* **1983**, *39*, 876.

[25] R. J. LeSuer, C. Buttolph, W. E. Geiger, *Anal. Chem.* **2004**, *76*, 6395–401.

[26] F. Barrière, N. Camire, W. E. Geiger, U. T. Mueller-Westerhoff, R. Sanders, *J. Am. Chem. Soc.* **2002**, *124*, 7262–7263.

[27] F. Barrière, W. E. Geiger, *J. Am. Chem. Soc.* **2006**, *128*, 3980–3989.

[28] G. Gritzner, J. Kuta, *Pure Appl. Chem.* **1984**, *56*, 461–466.

[29] A. Nafady, W. E. Geiger, *Organometallics* **2008**, *27*, 5624–5631.

[30] I. Noviandri, K. N. Brown, D. S. Fleming, P. T. Gulyas, P. A. Lay, A. F. Masters, L. Phillips, *J. Phys. Chem. B* **1999**, *103*, 6713–6722.